

NASA Contractor Report 3759

Developing Flow in S-Shaped Ducts

II - Circular Cross-Section Duct

A. M. K. P. Taylor, J. H. Whitelaw,
and M. Yianneskis

*Imperial College of Science and Technology
London, England*

Prepared for
Lewis Research Center
under Contract NASW-3435



National Aeronautics
and Space Administration

**Scientific and Technical
Information Office**

1984

TABLE OF CONTENTS

	Page
SUMMARY	1
1. INTRODUCTION	2
2. FLOW CONFIGURATION AND EXPERIMENTAL METHOD	2
2.1 FLOW CONFIGURATION	2
2.2 LASER-DOPPLER VELOCIMETER, EXPERIMENTAL METHOD AND MEASUREMENT TOLERANCES	3
3. RESULTS	6
3.1 LAMINAR FLOW RESULTS	6
3.2 TURBULENT FLOW RESULTS	6
4. DISCUSSION	8
5. CONCLUDING REMARKS	9
APPENDIX A - DETERMINATION OF BEAM PATH FOR STREAMWISE VELOCITY MEASUREMENTS	11
APPENDIX B - DETERMINATION OF BEAM PATH FOR r-COMPONENT VELOCITY MEASUREMENTS	17
APPENDIX C - TABULATED DATA, LAMINAR FLOW STREAMWISE VELOCITIES. REYNOLDS NUMBER 790, DEAN NUMBER = 299	21
APPENDIX D - TABULATED DATA, TURBULENT FLOW. REYNOLDS NUMBER = 48 000, DEAN NUMBER = 18 100	27
- TABLE I. MEAN & r.m.s. COMPONENTS OF STREAMWISE AND RADIAL VELOCITIES	27
- TABLE II. WALL PRESSURE DISTRIBUTION	33
APPENDIX E - DEFINITION OF SYMBOLS	35
REFERENCES	37
FIGURES	38

SUMMARY

The streamwise flow in a circular cross-section S-duct has been measured at four stations for Reynolds numbers of 790 and 48 000 (corresponding to Dean numbers of 299 and 18 100) in a water tunnel. The S-duct was formed from two 22.5° bends with 48 mm hydraulic diameter and 336 mm mean radius of curvature. The boundary layer at the inlet to the duct was approximately 25% of the hydraulic diameter in the laminar flow: in the turbulent flow it ranged from 10% to 20% around the periphery of the pipe. Laser-Doppler velocimetry was used to measure the streamwise velocity and, in turbulent flow, the associated fluctuation. For turbulent flow, the component of velocity at right angles to the duct centre-line and the wall pressures are also presented.

In the first bend, pressure-driven secondary flows are formed but are inferred to be larger in the laminar flow case. This is attributed to the thicker boundary layer thickness at the inlet. On passing into the second bend, the imposed radial pressure gradients give rise to forces which oppose the original streamwise vorticity, except for one region near the outer wall where the existing streamwise vorticity is sustained, according to the Squire-Winter formula for the generation of secondary flow, because of the local sign of the radial vorticity. In the turbulent flow the secondary flow on exit from the duct and remote from the pipe wall is found to be in the opposite direction to that in the first half.

The core flow, which is defined as fluid with a streamwise velocity greater than 0.90 of the maximum at any given streamwise location, migrates towards the outside wall of the first half of the bend and lies towards the inside wall of the second half for both Reynolds numbers. Comparison with measurements in a square cross-sectioned S-duct shows that the core's behaviour is generally similar, with small quantitative differences apparent only in the turbulent flow. This is because of the smaller secondary flows in the circular cross-section duct, attributable to the thinner inlet boundary layers.

An important objective of this work is to provide observations in sufficient detail and accuracy for the evaluation of numerical calculation methods. Accordingly, the measurements are presented in tabular form and are also available on magnetic tape from NASA Lewis Research Center for ease of reference.

1. INTRODUCTION

This report presents measurements of the streamwise and one cross-stream component of velocity in a S-duct of circular cross-section; it is the sequel to an investigation (reference 1) in a similar duct of square cross-section. Previous experimental investigations of the flow in S-ducts include observations for both fully-developed (reference 2) and thin (reference 3) inlet boundary layers, mainly in the form of total pressure measurements. In this work, the flow at the inlet to the S-duct had thin inlet boundary layers, with the purpose of the investigation being the measurement of the velocity characteristics by a laser-Doppler velocimeter. An important objective of this report is the recording of the velocity field in detail for the evaluation of numerical solutions of the equations of motion. The duct was of relatively mild curvature and small centre-line displacement so that there is little likelihood of flow separation at the walls of the duct. For this reason the flow should be particularly amenable to economical 'marching' solution techniques. Both laminar and turbulent flow have been investigated because the former permits the assessment of the numerical technique alone: the latter tests both the numerical technique and any 'turbulence model' which may be incorporated.

The velocities were measured using a laser-Doppler velocimeter but the effect of refraction at the curved duct walls requires a substantially different experimental procedure from that of reference 1. This is described in the following section and is followed by a presentation of the results for laminar and turbulent flow. The emphasis of the discussion in section 4 is in comparing and contrasting this flow with the results in the square cross-sectioned duct. The report closes with a list of concluding remarks.

2. FLOW CONFIGURATION AND EXPERIMENTAL METHOD

2.1 Flow configuration

The duct, shown schematically in figure 1, was assembled from two 22.5° sectors, each of which was manufactured by boring a solid Perspex block (n.b. Perspex is a polymethylmethacrylate plastic similar to Plexiglass). The ratio of the mean radius of curvature (336 mm) to the hydraulic diameter (48.0 ± 0.1 mm) was 7.0. The co-ordinate system, also shown in figure 1, is identical to that of reference 1. Streamwise location is denoted either by distance (X_H) along the duct centre-line (expressed in hydraulic diameters, with origin at the upstream face of the duct) or by the total angle turned through by the duct (θ). It is noted that the radial direction always refers to the normal to the radius of curvature of the duct centre-line and not to the radius of the pipe.

The duct was inserted in the water tunnel shown in figure 2, downstream of a straight duct of 4.4 hydraulic diameters in length. The water tunnel was similar to that used in reference 1, although no boundary layer trip was incorporated downstream of the contraction (7.84:1). This was so as to retain the smallest possible boundary layers on entry to the duct. The experiments were conducted at Reynolds numbers of 790 and 48 000 (Dean numbers of 299 and 18 100) corresponding to bulk velocities (mass flow rate divided by cross-sectional area) of 16.4 mm s^{-1} and 1.00 m s^{-1} . The mass flow rates were measured by precision bore flow meters which were insensitive to changes in the viscosity of water for the range of temperatures (12°C to 17°C) over which experiments were made.

2.2 Laser-Doppler velocimeter, experimental method and measurement tolerances

The experimental procedure used in reference 1 for the measurement of velocity components lying in the plane of curvature of the bend (observation of the velocity at a point in three different directions) could not be applied because of the effects of refraction at the curved Perspex/water interface. Indeed, cross-stream components of velocity can only be measured along a diameter of the pipe: as a result, velocity cross-correlations could not be measured. This is not an important restriction, however, because it is known (reference 1) that cross-correlations such as \overline{uv} are uninfluential except in regions very close to the walls. Surveys of the streamwise component of velocity were therefore made by traversing the optical arrangement shown in figure 3(a) and applying a ray tracing analysis (given as appendix A) to correct for the effects of refraction on the position of measurement and on the velocimeter's transfer constant (Doppler frequency to velocity).

Profiles of radial velocity were measured in the direction normal to the plane of curvature of the S-duct with the optical arrangement depicted in figure 3(b). As for the streamwise measurements, a ray tracing analysis (given as Appendix B) was used to correct for the effects of refraction.

Since the radial component of velocity is always small in comparison with the local streamwise component, it is necessary to use 'frequency shifting' (see reference 4) to generate a measurable Doppler signal. This shift was provided by the rotation of a radial diffraction grating (Institute for Applied Physics, TNO-TH {Netherlands}, type H) at a nominal speed of 448 r.p.m., corresponding to a frequency shift of 0.24 MHz. The relatively large value of the shift, as compared to the Doppler frequency corresponding to the radial velocities present in the duct, restricted accurate measurement of this component to the higher Reynolds number case.

The optical arrangement of the velocimeter and the electronic signal processing were virtually identical to those used in reference 1 and only the principal characteristics of the optical arrangement are summarised in the following table, for convenience.

Principal optical characteristics of the laser-Doppler velocimeter

Focal length of	
(a) lens nearest laser	200 mm
(b) collimating lens	300 mm
(c) imaging lens	200 mm
(d) objective lens	127 mm
Half angle of intersection (in air)	9.26 degrees
Laser light wavelength	632.8 nm
Fringe separation	1.97 μ m
Intersection volume dimensions, calculated at $1/e^2$ intensity level (in air) :	
(a) length	1.03 mm
(b) diameter	0.17 mm
Calculated number of fringes in measuring volume	85
Photomultiplier pinhole size	0.36 mm
Transfer constant	0.508 MHz/(m/s)
Nominal frequency shift (V-component only)	0.24 MHz

The flows were seeded (see reference 4) with minute dilutions of milk (about 20 ml in 10^4 litres) to increase the scattering-particle concentration.

Wall static pressures were measured, through tappings let into the wall of the duct, by a differential micromanometer.

Because the experimental procedure in this report is somewhat different to that of reference 1, the estimates of the tolerances in the measured quantities are also different. The following table summarizes these estimates.

Measurement errors

Quantity	Systematic error	Random error
X_H	1 mm	± 0.02 mm
r^*, z^*	0.5 mm	± 0.02 mm
θ	1.5 degrees	$\pm 0.4^\circ$
ϕ	0.05 degrees	nil
V_b (laminar)	1 %	± 1 %
V_b (turbulent)	nil	$\pm 3/4$ %
U	up to $0.02 V_b$	± 1 %
V	up to $0.04 V_b$	± 1 %
\tilde{u}	up to $0.02 V_b$	up to 3 %
\tilde{v}	up to $0.02 V_b$	up to 3 %
C_p	less than 1 %	± 0.017

- n.b. (a) Quantity ' θ ' refers here to the direction of the local tangent to the duct centre-line.
 (b) There is no systematic error in V_b (turbulent) because the flow meter has been independently calibrated.
 (c) Percentage errors refer to errors in local value.

The possible errors due to the refraction at the curved surfaces are of two kinds. The first is due to inaccuracies in the values of the dimensions of the test section, or the refractive indices of the media, which have been used in the calculations in appendices A and B. These are likely to be very small, however, and unimportant in comparison with the tolerances given in the table above. The second is due to residual surface scratches on the Perspex duct walls, remaining after the polishing of the plastic, which might reduce the coherence of the laser beams. Since good Doppler signals were obtained throughout the experiment, it appears that this source is also negligible.

In applying frequency shifting for the measurement of the V -component of velocity there are two potential sources of error. The first is associated with the accuracy with which the mean rotational speed of the grating (which is directly proportional to the frequency shift) is known. The rotational speed of the grating was measured by frequency counting and is accurate to much better than $0.01 V_b$. The second source is the short term (r.m.s.) instability of the rotation of the grating: this has been estimated as $0.005 V_b$ (reference 1) and hence both these sources are negligible compared to those already quoted in the table above.

3. RESULTS

3.1 Laminar flow results

Flow visualisation (by a combination of the hydrogen bubble technique and a plane of laser light) confirmed the laminar, steady nature of the flow. Careful observation of the outside wall of the first half of the bend revealed no evidence of any flow separation due to the adverse pressure gradient which exists there. Sample measurements (in both the laminar and turbulent flow regimes) on either side of the symmetry plane showed that the flow was symmetrical to within the precision of the measurements.

The streamwise velocities, normalised by the bulk velocity V_b , are shown in contour form in figure 4. There are four stations (1,3,4 and 5) which correspond closely with the stations in reference 1. Measurements were not made for the location of station 2 in reference 1 since the change, relative to station 1, is quite small. The contours have been drawn from points linearly interpolated from the measurement grid. In those regions where the position of the contour is conjectural, the contour is drawn as a dotted line.

In common with the results of reference 1, the boundary layer thickness (defined at 0.95 of the maximum velocity) is about one quarter of the hydraulic diameter at the beginning of the S-duct. A useful method for comparing the results of this work with those of reference 1 is to compare the location of the high-speed core of the flow, defined as that fluid which has streamwise velocity greater than, say, 0.90 of the maximum at any given station. This core behaves in the same way as for the square cross-sectional bend, namely that it is displaced to the outside wall in the first half of the S-duct due to the induced secondary motions and remains at $r^* \approx 0.3$ in the second half of the duct. By the outlet of the bend there is a large accumulation of low speed fluid near the outside wall of the second bend, which was also noted in reference 1, with an extensive region ($r^* \geq 0.5$, $z^* \leq 0.6$) where $\partial U / \partial z^*$ is positive. As noted in reference 1 and 2 the importance of this region in the second half is that it provides a source of secondary (i.e. streamwise vorticity) motion which is of the same sense as that established by the first half of the S-duct and thus continues the accumulation of low speed fluid which was begun in the first half of the S-duct. This is in contrast to regions where $\partial U / \partial z^*$ is negative (in other words, the wall boundary layers) which generate streamwise vorticity of a sense which attenuates the secondary flow set up by the first half of the S-duct.

The measurements are tabulated in appendix C.

3.2 Turbulent flow results

Flow visualisation of the turbulent flow was also carried out at the outside wall of the first half of the S-duct. Again, no evidence of flow separation was observed although it should be stated that observation of this region is substantially more difficult because of the high flow velocities.

The streamwise isotachs for the turbulent flow are depicted in figure 5, with values normalised by the bulk velocity, V_b . The boundary layers are, as expected, thinner than for the laminar flow and vary from 0.10 to 0.20 of the hydraulic diameter around the periphery of the pipe. This range is slightly thinner than that of the turbulent flow in the square cross-sectioned S-duct of reference 1, because of the shorter upstream tangent and the absence of a boundary layer trip. The core flow at station 1 is displaced towards the inside of the first half of the S-duct more markedly than for the corresponding station of the square cross-sectioned S-duct (reference 1). Although the core migrates towards the centre of the pipe by station 3, there is little evidence of any accumulation of low speed fluid at the inside wall, indicating weak secondary motion. The boundary layer in the round duct remains slightly thinner than in the square duct at the same station. On passing into the second half of the S-duct, the core is again displaced towards the inside surface and this displacement persists to the exit plane of the S-duct. The persistence of this displacement is, once again, more pronounced than in the case of the square cross-sectioned duct (reference 1). As in the case of the laminar flow, a region of positive $\partial U / \partial z^*$ exists near the outside of the second half of the duct which strengthens the existing secondary motion in accumulating low streamwise velocity fluid. It can be seen, for example, by noting the relative positions of the $U = 0.7 V_b$ contour, that low-speed fluid is more extensively distributed in the case of the circular, rather than square, cross-sectioned duct.

The profiles of V-component velocity in the z^* direction (for $r^* = 0.5$) are given in figure 6. The magnitudes at the entry to the duct are extremely small (about $0.02 V_b$) and in the direction of the displacement of the core of the streamwise isotachs. By the inflection plane (station 3) components of about $-0.05 V_b$ are observed in the core flow region with a measured maximum of about $+0.12 V_b$ near the wall. These values are smaller than those ($-0.09 V_b$ and $+0.13 V_b$) in the square-sectioned duct. In the second half of the duct the magnitudes decrease, and in the core flow eventually reverse, as a result of the change in the direction of the curvature of the S-duct. The importance of this change is well illustrated by the centre-line profile of radial velocity (figure 7), which clearly shows the abrupt alteration in the development on passing from the first to the second half of the duct. In reference 1 it was observed that negative components of V-velocity occur near the wall at station 5, but this is not evident here. This is consistent with the generally smaller secondary flows in this duct, although it is possible that negative components exist at locations closer to the wall than the extent of the measurements. It should also be recalled that the magnitudes of velocity which are under consideration are comparable to the systematic error of the velocimeter.

The streamwise variation in the wall static pressure around the pipe is presented in figure 8. The form of the graphs is similar to, if somewhat smaller than, those occurring in the square-sectioned S-duct of reference 1.

The turbulence levels for the streamwise component of velocity are shown as contour levels in figure 9 and as cross-stream (z^*) profiles for the \bar{v} component in figure 6. The turbulence level in the core is low

($\bar{u} \approx \bar{v} \approx 0.02 V_b$), as would be expected of the unstrained part of the flow, and higher values occur within the wall boundary layers. Qualitative agreement with reference 1 is good, although the 'pocket' of comparatively high turbulence which is observed at $r^* \approx 0.8$, $z^* \leq 0.4$ for stations 4 and 5 is absent from the square cross-sectioned duct. Its occurrence here is the corollary of the more extensive region of low momentum fluid in the vicinity of the outside of the second bend (comp. above).

The mean and r.m.s. velocities are tabulated in appendix D as table I and the wall pressure measurements as table II.

4. DISCUSSION

Developing flows in ducts can be discussed, at least qualitatively, in terms of streamwise acceleration and deceleration, brought about by the impressed streamwise pressure distribution, and cross-stream convection of streamwise momentum, due to secondary flows. These two mechanisms are, in many cases, competing ones in that the pressure distribution acts so as to accelerate the flow on the inside of a bend whereas streamwise vorticity (i.e. secondary flow) convects the low-speed boundary layer to the inside of the bend, thereby displacing the high speed core away from this region. The exclusion of the effects of shearing stresses (whether laminar or turbulent) from the discussion is not to deny their importance (see, for example, the numerical experiments of reference 6) but their influence does not introduce any qualitatively new features.

A simple analytical expression for the generation of streamwise vorticity is (reference 7)

$$\delta\omega_s = 2 \omega_r \delta\theta \quad (1)$$

where

$$\omega_s = \frac{\partial W}{\partial r'} - \frac{\partial V}{\partial z} \quad (2a)$$

and

$$\omega_r = \frac{\partial W}{\partial \theta} - \frac{\partial U}{\partial z} \quad (2b)$$

are the streamwise and radial components of vorticity, respectively, W is the velocity component in the z direction and r' is the radial co-ordinate directed towards the centre of curvature in each bend. Since $\partial W / \partial \theta \ll \partial U / \partial z$, equation (1) states that the magnitude of the streamwise vorticity which is generated depends on the value of $\partial U / \partial z$ or, what is equivalent in this case, the boundary layer thickness. In the laminar flow, this thickness was similar for both circular and square cross-sectioned S-ducts so that the behaviour of the core flow is virtually identical. In contrast, the boundary layer in the turbulent flow was thinner at the inlet to the circular cross-sectioned S-duct, with the result that the generation of streamwise vorticity is also smaller. Hence the flow is more influenced by the streamwise pressure gradient than by secondary flows and thus the behaviour of the core flow resembles that of a potential flow more closely than was the case for the square cross-sectioned S-duct.

5. CONCLUDING REMARKS

1. This report presents, in detail, the velocity characteristics of laminar and turbulent developing flow in a S-duct formed from two 22.5° sectors of a bend of circular cross-section, with a radius ratio of 7.0.
2. Pressure-driven secondary flows arise in the first half of the S-duct with a measured maximum of about 0.12 of the bulk velocity in turbulent flow. On passing through the second half of the S-duct the secondary flow established upstream is attenuated near the pipe walls, and reversed in the core flow region.
3. In common with observation in the square cross-sectioned S-duct, there is a region near the outside wall of the second half of the S-duct where the local sign of the radial vorticity results in a secondary flow which sustains that established upstream. This leads to a substantial local redistribution of the streamwise isotachs.
4. The laminar flow development is similar in both the circular and square cross-sectioned ducts. In the turbulent flow, the core flow in the case of the circular cross-sectioned S-duct lies closer to the inside wall of each half of the S-duct. It is argued that this is the result of thinner boundary layers at the entrance to the duct, as compared with the square cross-sectioned duct.
5. This report presents benchmark measurements against which the results of numerical calculation methods can be compared.

Note: The author's names are in alphabetical order.

APPENDIX A

DETERMINATION OF BEAM PATH FOR STREAMWISE VELOCITY MEASUREMENTS

A 1. PROBLEM STATEMENT

The position of the intersection of the two laser beams, and the angle with which the intersection occurs, are functions of the traverse co-ordinates because of the effects of refraction at the Perspex/air and Perspex/water interfaces. The half-angle of intersection (β) is a quantity of interest because of the dependence of the transfer constant (K) of the velocimeter on this angle:

$$U(t) = Kf(t) \quad \text{A 1(a)}$$

$$\text{where } K = \frac{\lambda/n}{2\sin(\beta)} \quad \text{A 1(b)}$$

Here $U(t)$ and $f(t)$ are the instantaneous values of streamwise velocity component and Doppler frequency, respectively and λ and n are the wavelength of laser light and the refractive index of the medium in which the beam intersection takes place. The purpose of this Appendix is to determine, by calculation, the position of the intersection and the angle β as a function of the traverse co-ordinates of the optical bench. The analysis is derived below in detail for the first half of the S-duct and the changes which are required for the second half are briefly described under a separate heading.

A 2. ANALYSIS FOR THE FIRST HALF OF THE S-DUCT

Figure A1 shows the attitude of the laser-Doppler velocimeter (LDV) for the measurement of streamwise velocity at any streamwise station within the first half of the S-duct. Let the (orthogonal) traverse directions of the optical bench be x and y , with origin as shown; both of these quantities are measured. The origin of co-ordinates for position relative to the duct, r and z , is also shown. In plan view, the optical axis of the LDV strikes the duct symmetrically and thus it is sufficient to determine the path of one beam only. The beams enter the Perspex wall at point A and are refracted at this interface to point B, the Perspex/water interface. Beam intersection takes place within the water at point C. The analysis proceeds by considering the problem in three stages: refraction at the air/Perspex interface, refraction at the Perspex/water interface and finally the beam path within water.

Refraction at the air/Perspex interface at point A

The beam is incident at angle a , found as follows. Let F be the virtual focus of the unrefracted laser beam and G the point on the axis of the generator of the S-duct which contains point A. Considering triangle AGF, the sine rule gives

$$\frac{\sin(a)}{R_a - y} = \frac{\sin(\pi - \phi)}{R_a} \quad A 2$$

where R_a is the radius of the outer air/Perspex interface and ϕ is the half-angle of beam intersection in air. Hence angle a can be found and the angle of refraction, b , can be found from Snell's law

$$n_a \sin(a) = n_p \sin(b) \quad A 3$$

where n_a and n_p are the refractive indices of air and Perspex respectively.

Refraction at the Perspex/water interface at point B

The refraction at this point is best analysed using vector algebra. The components of these vectors are resolved relative to a dextral system of co-ordinates, shown in figures A1 and A2, with origin at point B with \underline{i} , \underline{j} and \underline{k} being the unit vectors in the direction of the axes of the co-ordinate system.

The direction of the incident beam is given by \hat{p} (a unit vector). Its direction is determined by the angle γ . This angle is found from its complementary angle, u , by application of the sine rule to triangle ABG:

$$\gamma = \pi - u \quad A 4(a)$$

$$\frac{\sin(u)}{R_a} = \frac{\sin(b)}{BG} \quad A 4(b)$$

with the length BG, from figure A1 and A3

$$BG = R + \left(\frac{d}{2}\right) \cos(\epsilon) \quad A 4(c)$$

$$\text{where } \epsilon = \arcsin\left(\frac{x}{d/2}\right), \text{ from figure A3} \quad A 4(d)$$

Here R is the radius of curvature of the centre-line of the S-duct and d is the diameter of the pipe.

$$\text{Hence } \hat{p} = \cos\left(\frac{\pi}{2} - \gamma\right)\underline{i} + \cos(\gamma)\underline{j} + 0 \underline{k} \quad A 5$$

Refraction takes place about the normal to the Perspex/water interface at point B, with direction given by \underline{r} (a unit vector) increasing from the incident to the transmitting medium. Its direction is defined by angle ϵ (equation A4 (d)) and hence

$$\hat{r} = 0 \underline{i} + \cos(\epsilon)\underline{j} - \cos\left(\frac{\pi}{2} - \epsilon\right)\underline{k} \quad A 6$$

The direction of the refracted beam is denoted by \hat{q} (a unit vector) and is set by refraction: it is a required quantity. Let x_p denote the angle of inci-

dence: its value is given by

$$\cos(x_p) = \underline{\hat{p}} \cdot \underline{\hat{r}} \quad A 7$$

by definition of the vector scalar product and noting that both $\underline{\hat{p}}$ and $\underline{\hat{r}}$ are unit vectors. If x_w denotes the angle of refraction then, applying Snell's law,

$$n_w \sin(x_w) = n_p \sin(x_p) \quad A 8$$

which allows x_w to be found. The direction of $\underline{\hat{q}}$ can now be found, since the laws of refraction require that the refracted ray lies in the plane of incidence. The vectorial representation of this statement is (reference 8, p. 65, equation 4.8)

$$n_w \underline{\hat{q}} = (n_w \cos(x_w) - n_p \cos(x_p)) \underline{\hat{r}} + n_p \underline{\hat{p}} \quad A 9$$

Beam path within water

It is convenient for the subsequent analysis to find the direction of the line BD (figure A1). Let this be denoted by $\underline{\hat{s}}$ (a unit vector), which lies in the plane defined by \underline{i} and \underline{j} , and is determined (figures A2, A1) by the angle BDG (angle η). From figure A1

$$\eta = \rho - \zeta \quad A 10(a)$$

where

$$\rho + a = \phi \quad A 10(b)$$

(external angle of triangle AFG equals the sum of interior opposites)

and

$$\zeta + b = \gamma \quad A 10(c)$$

(external angle of triangle ABG equals the sum of interior opposites). Since angles a , ϕ , b and γ are known from the preceding, angle η is also known. Hence

$$\underline{\hat{s}} = \cos(\eta) \underline{i} + \cos\left(\frac{\pi}{2} - \eta\right) \underline{j} + 0 \underline{k} \quad A 11$$

The half-angle of intersection, which is one of the required quantities of the analysis, can now be found. This angle, BCD, is denoted as β : referring to figure A4, if the angle DBC is α , then

$$\beta = \frac{\pi}{2} - \alpha \quad A 12$$

But α is the angle between vectors $\underline{\hat{q}}$ and $\underline{\hat{s}}$ and is given by

$$\cos(\alpha) = \underline{\hat{q}} \cdot \underline{\hat{s}} \quad A 13$$

and hence the angle β can be found.

The other quantity which is required is the position of the point of intersection (point C) relative to the origin of co-ordinates r and z , figure A 1.

r co-ordinate. From figure A 1,

$$r = (R + \frac{d}{2}) - (DG - CD \cos(\sigma)) \quad A 14(a)$$

where σ is the angle between line CD and the \underline{i} - \underline{j} plane and is as yet unknown.
Now

$$DG = BG \cos(\eta) \quad A 14(b)$$

from figure A 1, with BG and η given by equations A(4c) and A 10(a) above.
The length CD is

$$CD = BD \tan(\alpha) \quad A 14(c)$$

from figure A 4, with α known from equation A 13 and

$$BD = BG \sin(\eta) \quad A 14(d)$$

The angle σ is found as follows. From Figure A 4, the direction of line CD can be written as

$$\underline{t} = \underline{\hat{q}} - \underline{\hat{s}} \cos(\alpha) \quad A 15(a)$$

The vector defining the normal to the \underline{i} - \underline{j} plane is \underline{k} and, from the definition of angle σ

$$\underline{k} \cdot \underline{t} = |\underline{k}| |\underline{t}| \cos(\frac{\pi}{2} - \sigma) \quad A 15(b)$$

where $|\underline{k}| \equiv 1$ (unit vector) and $|\underline{t}|$ can be found from A 15(a). Hence σ can be found.

z co-ordinate. From figure A 1

$$z = x + CD \sin(\sigma) \quad A 16$$

Since x , CD (equation A 14(c)) and σ (equation A 15(b)) are all known, z can be found. This completes the analysis for the first half of the duct.

A 3. ANALYSIS FOR THE SECOND HALF OF THE S-DUCT

The analysis is exactly the same, mutatis mutandis, as for the first half of the duct. Accordingly, only a brief statement is made concerning the changes.

Refraction at the air/Perspex interface at point A

Referring to figure A5, equation A2 for the angle a becomes

$$\frac{\sin(\pi-a)}{R_i + y} = \frac{\sin(\phi)}{R_i} \quad A17$$

where R_i is the radius of the inner air/Perspex interface. The equation defining angle b , equation A3, is unaltered.

Refraction at the Perspex/water interface at point B

Equations A4(a), (b) and (c) defining angles γ , u and the length BG are re-written as follows:

$$\frac{\sin(\gamma)}{R_i} = \frac{\sin(\pi-b)}{BG} \quad A18(a)$$

$$BG = R - \left(\frac{d}{2}\right) \cos(\epsilon) \quad A18(b)$$

For this analysis, the angle u is unnecessary and ϵ is given by equation A4(d), as before. The refraction at point B is represented by figure A6 and by inspection the representation of vectors \hat{p} and \hat{r} , equations A5 and A6, are unaffected, as are the equations for x_p and x_w (equations A7 and A8). Hence vector \hat{q} , defined by equation A9, stands.

Beam path within water

Equation A10(a), for angle n , is unaltered, but the equation for ρ now reads

$$a = \rho + \phi \quad A19(a)$$

from triangle AFG and the equation for ζ now is

$$b = \zeta + \gamma \quad A19(b)$$

from triangle ABG. The direction of vector \underline{s} is

$$\hat{s} = \cos(n)\underline{i} - \cos\left(\frac{\pi}{2} - n\right)\underline{j} + 0\underline{k} \quad A20$$

and the change in sign in the \underline{j} component, relative to equation A11, is noted and is evident in figure A6. The equations for β (equation A12) and α (equation A13) remain unaltered for the second half of the duct.

r co-ordinate. From figure A 5

$$r = (DG + CD \cdot \cos(\sigma)) - (R - \frac{d}{2}) \quad A 21$$

which replaces equation A 14(a). The equations for lengths DG, CD and BD (A 14(b), (c) and (d)) are unaffected, as is the analysis for finding the angle σ (equations A 15(a) and (b)).

z co-ordinate. Equation A 16 holds for this case.

A 4. TYPICAL RESULTS

For the determination of the beam path in the S-duct, the following values were used:

Refractive index of air, n_a	1.00
Refractive index of water, n_w	1.33
Refractive index of Perspex, n_p	1.490
Angle of intersection in air, ϕ	9.26 degrees
Radius of curvature of outer surface, R_a	377.70 mm
Radius of curvature of inner surface, R_i	293.97 mm
Radius of curvature of bend centre-line, R	336.00 mm
Diameter of pipe, d	48.00 mm

The two graphs in figure A 7 depict the change in the transfer constant (relative to that in air) of the LDV, ΔK , and the position of the beam intersection, r , both as a function of the radial traverse co-ordinate, y , for the first half of the duct. Both graphs compare the values for zero elevation ($z^* = 0.0$) with those obtaining at $z^* = -0.63$ and show that the influence of elevation on $\Delta K(y)$ and $r(y)$ is extremely small.

APPENDIX B

DETERMINATION OF BEAM PATH FOR r-COMPONENT VELOCITY MEASUREMENTS

B 1. PROBLEM STATEMENT

The position of the intersection of the two laser beams of the laser-Doppler velocimeter (LDV), and the angle with which this intersection takes place, are functions of the traverse co-ordinate in the same way as for appendix A. It is the purpose of this appendix to determine these two quantities by calculation. The problem is restricted to the case where the axis of symmetry of the LDV coincides with the vertical diameter of the pipe: that is the r co-ordinate is always $r=d/2$, where d is the diameter of the pipe. The analysis which follows is based on that of reference 9.

B 2. ANALYSIS

Figure B1 shows the attitude of the LDV for the measurement of r-component velocity at any streamwise location of the S-duct. The traverse distance of the optical bench is t, with origin of traverse taken as that position at which the beam intersection occurs at the Perspex/water interface. The optical axis of the LDV strikes the cross-section symmetrically and it is therefore sufficient to determine the path of one beam only. The beams enter the Perspex wall at point A (or A') and are refracted to point B (or B'), the Perspex/water interface: beam intersection takes place at point C within the water. Analysis proceeds by considering the displacement of point E' (the virtual focus of beam A' B') given a traverse movement t and from this calculates the position of point C.

Refraction at the air/Perspex interface

Let D be the virtual focus of the undisturbed laser beam when the traverse is positioned such that intersection occurs at the Perspex/water interface. Suppose the optical bench to be raised by a distance t as shown in the figure. The beam path is now A' B' and E' is the virtual focus of the beam as it propagates through the Perspex: it is required to find the distance BE', denoted as x. If the angle FBG is a right angle, then

$$\begin{aligned} FB &= AA' & B1 \\ A'A &= t \cdot \tan(\phi) \end{aligned}$$

and

where ϕ is the half-angle of beam intersection in air and which is known from measurement. The angle FE'B is equal to the angle (a) of refraction at point A' which, by Snell's law, is given by

$$n_a \sin(\phi) = n_p \sin(a) \quad B2$$

where n_a and n_p are the refractive indices of air and Perspex respectively. From triangle FE'B

$$x = \frac{FB}{\tan(a)} = \frac{t \cdot \tan(\phi)}{\tan(a)} \quad B3$$

Refraction at the Perspex/water interface

Two cases are distinguished. If

$$x \leq \frac{d}{2} \quad B 4$$

where d is the diameter of the pipe then the beam path is as shown in figure B1. The beam is incident at an angle b to the normal and is found by applying the sine rule to $B'E'G$:

$$\frac{E'G}{\sin(b)} = \frac{B'G}{\sin(\pi-a)} \quad B 5(a)$$

that is

$$\frac{(\frac{d}{2} - x)}{\sin(b)} = \frac{(d/2)}{\sin(\pi-a)} \quad B 5(b)$$

The angle of refraction is c and is given by Snell's law

$$n_p \cdot \sin(b) = n_w \cdot \sin(c) \quad B 6$$

The half-angle of intersection of the beams, β , which is one of the required quantities, is

$$\beta = \text{angle } (B'E'B) + \text{angle } (CB'E') \quad B 7(a)$$

since external angle of triangle $B'CE'$ is equal to the sum of interior opposites. Since

$$\begin{array}{ll} \text{angle } (B'E'B) &= a \quad B 7(b) \\ \text{and} \quad \text{angle } (CB'E') &= c-b \quad B 7(c) \\ \text{then} \quad \beta &= a+c-b \quad B 7(d) \end{array}$$

The location (z) of the point (C) of the intersection of the beams can now be found by application of the sine rule to triangle $B'CG$.

$$\frac{|z|}{\sin(c)} = \frac{(d/2)}{\sin(\pi-\beta)} \quad B 8$$

where $|z|$ denotes the magnitude of z .

If

$$x > \frac{d}{2} \quad B 9$$

then the beam path is as shown in figure B2. Equation B5(a), from which the angle b is found, is now

$$\frac{(x-d/2)}{\sin(b)} = \frac{(d/2)}{\sin(a)} \quad B 10$$

The angle of refraction, c , is unaltered (equation B6). The half angle of

intersection is

$$\begin{aligned}\beta &= \text{angle } (GE'B) - \text{angle } (E'B'C) & B11(a) \\ \text{angle } (GE'B) &= a & B11(b) \\ \text{angle } (E'B'C) &= c-b & B11(c) \\ \beta &= a-(c-b) & B11(d)\end{aligned}$$

hence

The location of point C is now given by

$$\frac{z}{\sin(c)} = \frac{(d/2)}{\sin \beta} \quad B12$$

B 3. TYPICAL RESULTS

The graph in figure B3 depicts the change in the transfer constant (relative to that in air for $\phi = 9.11$ degrees) of the LDV, ΔK , as a function of the position of the measuring volume, z^* . The change in this quantity is much greater than was the case for the streamwise measurements, detailed in Appendix A and is partly due to the larger angles of incidence which occur. However it is noted that even when the measuring volume lies at the centre of the duct ($z^* = 0$), and hence there is no refraction at the Perspex/water interface at point B', there is an increase of about 12% in K over the value obtaining in air. This is due to the change (from 632.8 nm in vacuo) in wavelength of the laser light because of the refractive index of water ($n_w = 1.33$) as well as refraction at the air/Perspex interface at A'.

APPENDIX C

TABULATED DATA

22.5°/22.5° S-DUCT, CIRCULAR CROSS-SECTION
LAMINAR FLOW STREAMWISE VELOCITIES (REYNOLDS
NUMBER = 790, DEAN NUMBER = 299, BULK VELOCITY
= 16.4 mm/s)

- Notes: (1) 'THETA' is angle of turning of bend,
measured from S-duct inlet.
- (2) 'R' and 'Z' are cross-stream co-
ordinate directions, defined in
figure 1.
- (3) 'U' is the streamwise component of
velocity.

LAMINAR FLOW STREAMWISE VELOCITIES-STATION 1. THETA=2.25 DEGS.

R(MM) :	4.41	6.98	10.82	15.91	20.96	25.98	30.96	35.91	40.82	44.48
Z(MM) :	-0.00	-0.00	-0.00	-0.00	-0.00	-0.00	-0.00	-0.00	-0.00	-0.00
U(MM/S) :	11.12	17.45	22.88	25.88	26.46	26.44	26.73	25.13	20.03	13.53
R(MM) :	4.66	7.23	11.06	16.14	21.19	26.20	31.18	36.13	41.04	44.70
Z(MM) :	-5.11	-5.17	-5.27	-5.41	-5.54	-5.67	-5.80	-5.93	-6.05	-6.15
U(MM/S) :	11.87	18.25	22.81	25.01	25.46	25.52	25.08	22.94	18.26	12.36
R(MM) :	5.09	7.65	10.20	12.75	17.81	22.83	27.83	32.78	37.71	40.16
Z(MM) :	-10.16	-10.31	-10.46	-10.60	-10.83	-11.17	-11.45	-11.74	-12.01	-12.15
U(MM/S) :	8.45	15.07	19.65	21.51	24.44	25.08	24.81	22.42	16.64	11.79
R(MM) :	6.06	8.62	11.16	13.70	18.74	23.75	28.73	31.21	33.67	36.13
Z(MM) :	-12.70	-12.89	-13.08	-13.28	-13.66	-14.05	-14.43	-14.62	-14.80	-14.99
U(MM/S) :	5.56	11.60	16.39	19.27	21.90	22.89	22.21	19.96	17.38	13.86
R(MM) :	7.65	10.19	12.73	15.25	20.27	25.25	30.21	32.67	35.13	37.57
Z(MM) :	-15.24	-15.50	-15.76	-16.02	-16.54	-17.05	-17.55	-17.80	-18.05	-18.30
U(MM/S) :	4.96	10.01	14.07	16.90	19.53	19.18	16.20	12.96	8.70	3.73
R(MM) :	11.76	14.27	16.77	19.27	22.93	27.94	30.39			
Z(MM) :	-18.09	-18.45	-18.81	-19.16	-19.63	-20.39	-20.74			
U(MM/S) :	6.49	9.39	11.64	12.88	13.23	10.35	7.45			

41.38
-12.22
8.78

38.58
-15.18
9.47

41.03
-15.36
3.25

LAMINAR FLOW STREAMWISE VELOCITIES: STATION 3. THETA=20.25 DEGS.

R(MM)	2.48	5.05	7.62	10.18	15.27	20.33	25.35	30.34	34.06	36.52	38.98	41.43	43.88
Z(MM)	-	-	-	-	-	-	-	-	-	-	-	-	-
U(MM/S)	13.30	23.25	26.00	26.57	26.86	26.89	25.66	22.99	17.59	14.20	11.52	8.83	5.95
R(MM)	3.24	5.82	8.38	10.93	16.02	21.07	26.08	31.06	34.77	37.23	39.69	42.14	44.58
Z(MM)	-	-	-	-	-	-	-	-	-	-	-	-	-
U(MM/S)	14.66	22.80	24.64	25.94	26.77	26.64	25.30	20.60	15.88	13.06	10.31	7.29	3.88
R(MM)	4.51	7.07	9.63	12.18	17.24	22.27	27.27	32.23	35.93	38.38	40.83	43.28	45.73
Z(MM)	-	-	-	-	-	-	-	-	-	-	-	-	-
U(MM/S)	9.94	17.81	21.58	23.92	25.98	25.28	22.65	17.32	12.68	9.10	5.21	1.32	-2.13
R(MM)	6.25	8.81	11.35	13.89	18.93	23.94	28.92	33.86	36.32	38.77	41.22	43.67	46.12
Z(MM)	-	-	-	-	-	-	-	-	-	-	-	-	-
U(MM/S)	11.85	19.11	22.97	24.34	24.91	23.46	19.40	13.33	9.78	6.23	2.68	-0.87	-3.32
R(MM)	8.80	11.33	13.86	16.38	21.39	26.37	31.32	36.23	40.14	44.05	47.96	51.87	55.78
Z(MM)	-	-	-	-	-	-	-	-	-	-	-	-	-
U(MM/S)	11.94	17.67	20.43	22.16	21.93	19.43	13.73	9.44	4.77	0.10	-4.55	-9.20	-13.85
R(MM)	12.45	14.96	17.46	21.20	24.91	28.61	31.07	33.53	36.23	38.98	41.73	44.48	47.23
Z(MM)	-	-	-	-	-	-	-	-	-	-	-	-	-
U(MM/S)	10.99	14.81	16.69	17.11	15.07	10.70	-20.83	-6.50	8.83	13.06	17.29	21.52	25.75

LAMINAR FLOW STREAMWISE VELOCITIES: STATION 4. THETA=22.5+9.0 DEGS.

R(MM) :	2.00	4.10	6.92	11.17	16.89	19.77	22.66	28.49	34.38	40.34	43.34
Z(MM) :	-1.00	-1.00	-1.00	-1.00	-1.00	-1.00	-1.00	-1.00	-1.00	-1.00	-1.00
U(MM/S) :	15.58	24.27	28.08	29.09	28.63	26.90	23.13	15.65	11.29	7.80	5.20
R(MM) :	2.41	4.51	7.33	10.16	14.44	20.18	25.99	31.86	37.78	43.77	
Z(MM) :	-5.05	-5.10	-5.18	-5.25	-5.36	-5.51	-5.66	-5.82	-5.97	-6.13	
U(MM/S) :	11.61	21.31	27.51	29.28	28.77	26.18	19.47	13.61	9.31	3.93	
R(MM) :	4.76	6.88	9.70	12.55	16.84	22.61	28.43	31.37	37.29	40.27	
Z(MM) :	-10.15	-10.27	-10.43	-10.59	-10.83	-11.16	-11.49	-11.66	-11.99	-12.16	
U(MM/S) :	11.94	22.00	26.77	28.13	28.15	25.14	20.17	18.35	11.80	6.04	
R(MM) :	6.95	9.78	12.62	15.47	21.23	25.58	29.96	34.38	38.83		
Z(MM) :	-12.76	-12.98	-13.20	-13.41	-13.85	-14.19	-14.52	-14.86	-15.20		
U(MM/S) :	13.52	23.30	26.36	27.23	26.30	23.12	20.70	15.28	6.26		
R(MM) :	8.63	11.46	14.30	20.03	25.82	30.20	34.62				
Z(MM) :	-15.34	-15.63	-15.92	-16.51	-17.10	-17.55	-18.01				
U(MM/S) :	11.44	19.59	24.46	25.63	23.30	17.89					
R(MM) :	11.14	13.97	16.82	22.56	28.35	31.27					
Z(MM) :	-18.01	-18.41	-18.81	-19.63	-20.45	-20.86					
U(MM/S) :	8.39	14.77	17.62	18.13	11.66	5.83					

LAMINAR FLOW STEPWISE VELOCITIES:STATION 5. THETA=22.5+20.25 DEGS.

R(MM) :	3.12	5.23	8.05	12.31	18.04	23.82	20.92	23.82	26.74	29.67	35.57	41.54	44.54
Z(MM) :	-7.00	-5.00	-3.00	-1.00	1.00	3.00	5.00	7.00	9.00	11.00	13.00	15.00	17.00
U(MM/S) :	7.21	13.47	24.34	30.24	29.08	20.63	25.75	20.55	16.07	14.06	11.98	10.00	6.54
R(MM) :	2.69	4.79	7.61	11.87	17.59	20.47	23.37	26.28	29.21	35.11	41.07	44.07	
Z(MM) :	-5.06	-5.11	-5.18	-5.30	-5.44	-5.52	-5.60	-5.67	-5.75	-5.90	-6.06	-6.14	
U(MM/S) :	6.77	13.85	22.37	28.99	28.32	24.76	21.30	17.22	15.70	16.19	10.87	4.78	
R(MM) :	4.62	6.74	9.59	13.83	19.57	22.46	25.37	28.29	31.22	37.14	40.12		
Z(MM) :	-10.14	-10.26	-10.42	-10.66	-10.99	-11.15	-11.32	-11.48	-11.65	-11.99	-12.15		
U(MM/S) :	7.87	14.66	22.76	28.32	27.77	25.83	23.19	21.34	20.90	18.31	10.93		
R(MM) :	5.68	7.80	10.63	14.90	20.65	26.45	32.32	35.27	38.24				
Z(MM) :	-12.67	-12.83	-13.04	-13.37	-13.81	-14.25	-14.70	-14.93	-15.16				
U(MM/S) :	7.24	13.89	21.25	27.59	27.60	25.07	22.76	18.78	10.56				
R(MM) :	7.85	9.97	12.81	17.09	22.85	28.67	31.60	34.54					
Z(MM) :	-15.26	-15.48	-15.77	-16.21	-16.80	-17.40	-17.70	-18.00					
U(MM/S) :	6.12	12.28	18.76	24.53	25.70	23.35	19.93	13.49					
R(MM) :	11.18	14.01	16.86	19.72	25.48	28.39	31.30						
Z(MM) :	-18.01	-18.41	-18.82	-19.22	-20.04	-20.45	-20.87						
U(MM/S) :	7.36	12.86	17.58	19.99	18.67	14.64	6.84						

APPENDIX D

TABULATED DATA

22.5°/22.5° S-DUCT, CIRCULAR CROSS-SECTION

TURBULENT FLOW : REYNOLDS NUMBER = 48 000

DEAN NUMBER = 18 100

BULK VELOCITY = 1.00 m/s

TABLE I

MEAN & r.m.s. COMPONENTS OF STREAMWISE AND
RADIAL VELOCITIES

- Notes: (1) 'THETA' is angle of turning of bend,
measured from S-duct inlet.
- (2) 'R' and 'Z' are cross-stream co-ordinate
directions, defined in figure 1.
- (3) 'U' is the time-mean streamwise component
of velocity and 'UD' is the corresponding
r.m.s. velocity fluctuation
- (4) 'V' is the time-mean radial component
of velocity and 'VD' is the corresponding
r.m.s. velocity fluctuation
- (5) 'XH' is distance along duct's centre-line
(in hydraulic diameters) with origin at
the duct inlet.

TURBULENT FLOW STREAMWISE VELOCITIES; STATION 1. THETA=2.25 DEGS

R(MM) :	2.86	5.44	8.01	13.11	18.18	23.22	28.22	33.19	38.12	43.02	45.46	
Z(MM) :	-.00	-.00	-.00	-.00	-.00	-.00	-.00	-.00	-.00	-.00	-.00	
U(M/S) :	.88	1.03	1.07	1.09	1.09	1.11	1.12	1.13	1.14	1.08	.98	
UD(M/S) :	.082	.039	.015	.011	.012	.010	.009	.010	.010	.049	.069	
R(MM) :	3.11	5.69	8.25	10.81	15.89	20.94	25.95	30.93	35.88	38.34	40.79	45.67
Z(MM) :	5.07	5.13	5.20	5.27	5.40	5.53	5.66	5.79	5.92	5.98	6.05	6.18
U(M/S) :	.88	1.00	1.07	1.09	1.09	1.11	1.11	1.12	1.13	1.13	1.12	1.11
UD(M/S) :	.075	.050	.017	.013	.011	.010	.012	.011	.012	.015	.030	.057
R(MM) :	4.64	7.20	9.76	12.30	17.37	22.40	27.39	32.35	37.28	39.73	42.17	
Z(MM) :	10.14	10.28	10.43	10.57	10.86	11.15	11.43	11.71	11.99	12.13	12.27	
U(M/S) :	.83	.99	1.05	1.08	1.09	1.10	1.11	1.10	1.06	1.01	.94	
UD(M/S) :	.085	.053	.026	.014	.011	.010	.011	.022	.043	.059	.071	
R(MM) :	5.87	8.42	10.97	13.51	16.03	21.06	26.06	31.02	33.49	35.95	38.40	40.84
Z(MM) :	12.68	12.88	13.07	13.26	13.46	13.84	14.22	14.60	14.79	14.98	15.16	15.35
U(M/S) :	.84	.97	1.04	1.06	1.08	1.10	1.10	1.10	1.08	1.02	.93	.80
UD(M/S) :	.101	.057	.037	.028	.020	.015	.013	.021	.036	.053	.068	.088
R(MM) :	7.15	9.69	12.22	14.74	19.77	24.76	29.71	32.18	34.64	37.08		
Z(MM) :	15.19	15.45	15.71	15.97	16.48	16.99	17.50	17.75	18.00	18.25		
U(M/S) :	.80	.94	.99	1.02	1.05	1.08	1.09	1.05	.98	.87		
UD(M/S) :	.091	.070	.060	.050	.040	.032	.034	.044	.064	.093		
R(MM) :	9.68	12.20	14.71	19.70	24.67	27.13	29.60	32.05				
Z(MM) :	17.80	18.16	18.51	19.22	19.93	20.28	20.62	20.97				
U(M/S) :	.77	.87	.91	.97	1.00	1.01	.97	.90				
UD(M/S) :	.101	.080	.070	.063	.060	.059	.066	.080				

TURBULENT FLOW STREAMWISE VELOCITIES; STATION 3. THETA=20.25 DEGS.

R(MM) :	2.54	5.12	7.69	10.25	12.80	17.87	27.91	30.40	32.88	35.35	37.81	40.27	42.72	45.15
Z(MM) :	- .00	- .00	- .00	- .00	- .00	- .00	- .00	- .00	- .00	- .00	- .00	- .00	- .00	- .00
U(M/S) :	.99	1.06	1.10	1.11	1.12	1.13	1.14	1.14	1.14	1.14	1.12	1.05	.93	.76
UD(M/S) :	.063	.049	.029	.014	.012	.011	.012	.013	.016	.018	.031	.048	.046	.077
R(MM) :	2.98	5.56	8.12	10.68	13.23	18.29	23.33	28.32	33.29	35.76	38.22	40.67	43.11	
Z(MM) :	5.06	5.13	5.20	5.26	5.33	5.46	5.59	5.72	5.85	5.92	5.98	6.05	6.11	
U(M/S) :	.96	1.03	1.09	1.12	1.13	1.13	1.14	1.15	1.15	1.13	1.09	1.01	.87	
UD(M/S) :	.069	.059	.032	.017	.013	.012	.012	.012	.018	.027	.041	.057	.075	
R(MM) :	4.96	7.52	10.08	12.62	15.16	20.20	25.21	30.19	32.66	35.13	37.59	40.04	42.48	
Z(MM) :	10.16	10.30	10.45	10.59	10.74	11.02	11.31	11.59	11.73	11.87	12.01	12.15	12.28	
U(M/S) :	.93	1.03	1.10	1.12	1.13	1.14	1.14	1.13	1.12	1.07	1.01	.93	.79	
UD(M/S) :	.079	.062	.038	.021	.014	.012	.014	.023	.032	.041	.051	.059	.071	
R(MM) :	5.93	8.49	11.03	13.57	16.10	21.13	23.63	28.61	32.32	34.78	37.24	39.68		
Z(MM) :	12.69	12.88	13.07	13.27	13.46	13.85	14.04	14.42	14.70	14.89	15.08	15.26		
U(M/S) :	.91	1.01	1.08	1.09	1.11	1.13	1.13	1.13	1.09	1.04	.96	.87		
UD(M/S) :	.077	.064	.042	.028	.019	.020	.018	.026	.040	.046	.056	.062		
R(MM) :	7.40	9.94	12.47	15.00	18.77	22.52	26.25	29.96	32.42	34.88	37.33			
Z(MM) :	15.22	15.48	15.74	16.00	16.38	16.77	17.15	17.53	17.78	18.03	18.28			
U(M/S) :	.92	1.00	1.05	1.05	1.09	1.07	1.07	1.05	1.01	.94	.83			
UD(M/S) :	.079	.067	.056	.052	.039	.045	.048	.054	.062	.066	.079			
R(MM) :	11.19	13.71	16.21	18.71	22.44	26.15	28.61	31.07	33.52					
Z(MM) :	18.01	18.37	18.73	19.08	19.61	20.14	20.49	20.83	21.18					
U(M/S) :	.93	.98	1.01	1.02	1.03	.98	.96	.89	.80					
UD(M/S) :	.079	.066	.066	.064	.061	.067	.072	.079	.089					

TURBULENT FLOW STREAMWISE VELOCITIES; STATION 4. THETA=22.5+9.0 DEGS.

R(MM) :	2.62	5.23	8.05	10.89	13.74	19.48	25.28	31.14	34.09	37.06	40.04	43.04
Z(MM) :	1.00	1.00	1.00	1.00	1.00	1.00	1.00	1.00	1.00	1.00	1.00	1.00
U(M/S) :	1.14	1.19	1.21	1.20	1.18	1.17	1.15	1.13	1.03	.86	.69	.54
UD(M/S) :	.051	.034	.019	.014	.013	.012	.014	.020	.051	.076	.083	.067
R(MM) :	4.23	6.34	9.17	12.01	17.73	23.52	29.36	32.30	35.26	38.23	41.22	44.22
Z(MM) :	5.10	5.15	5.23	5.30	5.45	5.60	5.75	5.83	5.91	5.98	6.06	6.14
U(M/S) :	1.15	1.16	1.20	1.19	1.17	1.16	1.13	1.10	1.00	.87	.74	.63
UD(M/S) :	.050	.044	.023	.013	.012	.012	.016	.033	.054	.065	.070	.065
R(MM) :	5.12	7.93	10.77	13.62	19.35	25.15	31.00	33.95	36.92	39.90	42.89	
Z(MM) :	10.17	10.33	10.49	10.65	10.97	11.30	11.64	11.80	11.97	12.14	12.31	
U(M/S) :	1.09	1.13	1.18	1.19	1.18	1.16	1.09	1.03	.95	.85	.72	
UD(M/S) :	.063	.049	.028	.016	.013	.013	.033	.043	.052	.058	.072	
R(MM) :	6.32	9.14	11.98	14.83	17.70	23.47	29.30	32.24	35.20	38.16	41.15	
Z(MM) :	12.71	12.93	13.15	13.36	13.58	14.03	14.47	14.70	14.92	15.15	15.38	
U(M/S) :	1.07	1.15	1.17	1.18	1.17	1.15	1.10	1.04	.96	.87	.73	
UD(M/S) :	.060	.052	.034	.020	.017	.022	.033	.044	.056	.065	.081	
R(MM) :	7.78	10.61	13.45	16.30	19.17	24.95	30.79	33.73	36.69			
Z(MM) :	15.26	15.55	15.84	16.15	16.42	17.02	17.61	17.92	18.22			
U(M/S) :	1.07	1.13	1.15	1.15	1.14	1.09	1.02	.95	.84			
UD(M/S) :	.072	.056	.044	.033	.036	.046	.060	.063	.075			
R(MM) :	10.01	12.84	15.68	18.54	21.41	27.19	30.10	33.02				
Z(MM) :	17.85	18.25	18.65	19.06	19.46	20.28	20.70	21.11				
U(M/S) :	1.03	1.09	1.10	1.10	1.08	1.01	.95	.85				
UD(M/S) :	.080	.060	.056	.052	.057	.061	.066	.080				

TURBULENT FLOW STREAMWISE VELOCITIES; STATION 5. THETA=22.5+20.25 DEGS.

R(MM) :	2.42	5.23	8.05	10.89	16.60	22.37	28.20	31.14	34.09	37.06	40.04	43.04
Z(MM) :	-0.00	-0.00	-0.00	-0.00	-0.00	-0.00	-0.00	-0.00	-0.00	-0.00	-0.00	-0.00
U(M/S) :	1.07	1.18	1.21	1.21	1.12	1.17	1.13	.99	.81	.67	.61	.58
UD(M/S) :	.074	.041	.027	.018	.012	.014	.035	.093	.104	.076	.060	.062
R(MM) :	3.39	6.20	9.03	10.45	14.72	17.59	23.37	29.21	32.15	35.11	38.08	41.07
Z(MM) :	5.07	5.15	5.22	5.26	5.37	5.44	5.60	5.75	5.82	5.90	5.98	6.06
U(M/S) :	1.03	1.16	1.19	1.20	1.13	1.19	1.18	1.15	1.06	.93	.84	.81
UD(M/S) :	.078	.046	.033	.024	.013	.013	.012	.025	.072	.089	.081	.062
R(MM) :	4.34	7.16	9.99	12.83	15.69	18.56	24.35	30.19	33.14	36.10	39.08	42.07
Z(MM) :	10.12	10.28	10.44	10.60	10.77	10.93	11.26	11.59	11.76	11.93	12.10	12.27
U(M/S) :	1.01	1.15	1.19	1.20	1.19	1.19	1.17	1.11	1.05	.98	.91	.81
UD(M/S) :	.085	.052	.034	.019	.015	.014	.017	.038	.048	.056	.059	.077
R(MM) :	5.61	8.43	11.27	14.12	16.98	19.85	25.65	31.51	34.46	37.42	40.40	
Z(MM) :	12.66	12.88	13.09	13.31	13.53	13.75	14.19	14.64	14.87	15.09	15.32	
U(M/S) :	1.01	1.14	1.17	1.19	1.19	1.18	1.15	1.07	1.02	.94	.78	
UD(M/S) :	.078	.049	.037	.024	.020	.021	.029	.046	.052	.064	.091	
R(MM) :	7.64	10.46	13.30	16.16	19.03	21.91	27.72	30.64	33.58	36.54		
Z(MM) :	15.24	15.53	15.82	16.11	16.41	16.70	17.30	17.60	17.90	18.20		
U(M/S) :	.98	1.11	1.16	1.16	1.17	1.14	1.09	1.04	.98	.88		
UD(M/S) :	.083	.060	.044	.036	.034	.039	.048	.054	.065	.082		
R(MM) :	10.29	13.12	15.97	18.82	21.69	27.48	30.39	33.32				
Z(MM) :	17.89	18.29	18.69	19.10	19.50	20.33	20.74	21.16				
U(M/S) :	.97	1.08	1.12	1.11	1.11	1.04	.98	.86				
UD(M/S) :	.079	.072	.057	.051	.051	.061	.071	.088				

TURBULENT FLOW RADIAL VELOCITIES; STATION 1. THETA=20.25 DEGS.

Z(MM) :	21.86	20.86	19.87	15.98	12.22	8.57	5.03	1.60	1.72
V(M/S) :	.02	.02	.03	.02	.02	.02	.02	.02	.02
VD(M/S) :	.053	.056	.051	.032	.018	.019	.019	.017	.016

TURBULENT FLOW RADIAL VELOCITIES; STATION 3. THETA=20.25 DEGS.

Z(MM) :	21.86	20.86	19.87	15.98	12.22	8.57	1.60	1.72
V(M/S) :	.13	.10	.07	.04	.04	.05	.05	.06
VD(M/S) :	.059	.055	.053	.040	.021	.017	.016	.018

TURBULENT FLOW RADIAL VELOCITIES; STATION 4. THETA=22.5+9.0 DEGS.

Z(MM) :	21.86	20.86	19.87	17.91	15.98	12.22	8.57	1.60	1.72
V(M/S) :	.08	.08	.07	.04	.02	.01	.00	.01	.01
VD(M/S) :	.056	.054	.050	.045	.035	.022	.019	.017	.017

TURBULENT FLOW RADIAL VELOCITIES; STATION 5. THETA=22.5+20.25 DEGS.

Z(MM) :	21.86	20.86	19.87	17.91	15.98	12.22	9.57	1.60
V(M/S) :	.02	.03	.04	.05	.04	.04	.03	.02
VD(M/S) :	.059	.051	.044	.038	.033	.020	.017	.016

TURBULENT FLOW RADIAL VELOCITIES; STREAMWISE CENTRELINE PROFILE

Z(MM) :	.76	.76	.76	.76	.76	.76	.76	.76	.76
V(M/S) :	-.02	-.03	-.03	-.05	-.08	-.08	-.02	-.01	-.00
VD(M/S) :	.017	.018	.019	.019	.018	.017	.017	.018	.017
XH	0.73	1.10	1.47	1.83	2.20	2.57	2.93	3.30	3.67

TABLE II
WALL PRESSURE DISTRIBUTION

Note : 'Pressure coefficient' is defined as

$$C_p \equiv \frac{(P - P_{\text{ref}})}{\frac{1}{2} \rho V_b^2}$$

where ρ is water density (1000 kg m^{-3})
 V_b is bulk velocity (1.00 m/s)

STREAMWISE STATION (X/H)	RADIAL POSITION (R)	SPANWISE POSITION (Z)	PRESSURE COEFFICIENT
-1.00	0.0	0.0	0.0 (REF)
	0.5	-1.0	-0.014
	1.0	0.0	-0.015
1.10	0.0	0.0	0.078
	0.5	-1.0	-0.050
	1.0	0.0	-0.203
2.20	0.0	0.0	0.042
2.38	0.5	-1.0	-0.079
	1.0	0.0	-0.203
3.30	0.0	0.0	-0.274
	0.5	-1.0	-0.137
	1.0	0.0	-0.038
4.40	0.0	0.0	-0.326
	0.5	-1.0	-0.153
	1.0	0.0	-0.053
6.50	0.0	0.0	-0.196
	0.5	-1.0	-0.204
	1.0	0.0	-0.190

APPENDIX E

DEFINITION OF SYMBOLS

Roman Characters

C_p	Pressure coefficient (figure 8)
D_H	Hydraulic diameter (48 mm)
De	Dean number: $De \equiv \left \frac{\frac{1}{2} D_H}{R} \right ^{\frac{1}{2}} \cdot Re$
P	Pressure at wall
P_{ref}	Reference value of P ($X_H = 0.0$, $r^* = 0$, $z^* = 0$)
r	Radial co-ordinate direction (figure 1)
r_i	Radius of curvature of suction surface
r_o	Radius of curvature of pressure surface
r^*	Normalised radial co-ordinate: $r^* \equiv \frac{r - r_o}{r_i - r_o}$
R	Mean radius of curvature: $R = \frac{1}{2} (r_i + r_o)$
Re	Reynolds number based on V_b and D_H
U	Velocity in streamwise direction
\tilde{u}	R.m.s. fluctuating velocity in streamwise direction
V	Velocity in radial direction
V_b	Bulk mean velocity (mass flow rate/duct area)
\tilde{v}	R.m.s. fluctuating velocity in radial (r) direction
W	Velocity in spanwise direction
X_H	Distance along duct centre-line, expressed in hydraulic diameters (origin lies at $\theta = 0^\circ$)
z	Spanwise co-ordinate direction (figure 1)
$z_{\frac{1}{2}}$	Duct half-width (24 mm)
z^*	Normalised spanwise co-ordinate: $z^* \equiv \frac{z}{z_{\frac{1}{2}}}$ (see figure 1)

Greek Characters

θ	Angle of turning in streamwise direction (see figure 1)
ϕ	Half-angle of beam intersection
ω_s	Streamwise component of mean vorticity (equation 1,2a)
ω_r	Radial component of mean vorticity (equation 1,2b)

REFERENCES

1. Taylor, A.M.K.P., Whitelaw, J.H. and Yianneskis, M. (1982). Developing flow in S-shaped ducts. Part I: Square cross-section duct. NASA CR-3550.
2. Rowe, M. (1970). Measurements and computations of flow in pipe bends. J. Fluid Mech., 43, part 4, 771-783.
3. Bansod, P. and Bradshaw, P. (1972). The flow in S-shaped ducts. Aeronautical Quarterly, 23, part 2, 131-140.
4. Durst, F., Melling, A. and Whitelaw, J.H. (1982). Principles and practice of laser-Doppler anemometry. Second Edition, Academic Press, London, England.
5. Melling, A. and Whitelaw, J.H. (1976). Turbulent flow in a rectangular duct. J. Fluid Mech., 78, part 2, 289-315.
6. De Vriend, H.J. (1981). Velocity redistribution in curved rectangular channels. J. Fluid Mech., 107, 423-439.
7. Scorer, R.S. (1978). Environmental Aerodynamics, Ellis Horwood, Chichester, England.
8. Hecht, E. and Zajac, A. (1974). Optics. Addison-Wesley Publishing Co., Reading, Massachusetts, U.S.A.
9. Kirmse, R. (1974). Optische Probleme bei der Anwendung des Laser-Doppler Anemometers zur Messung von Strömungsgeschwindigkeiten in Flüssigkeiten. Archiv für technisches Messen, Blatt V, 1246-1, 41-46.

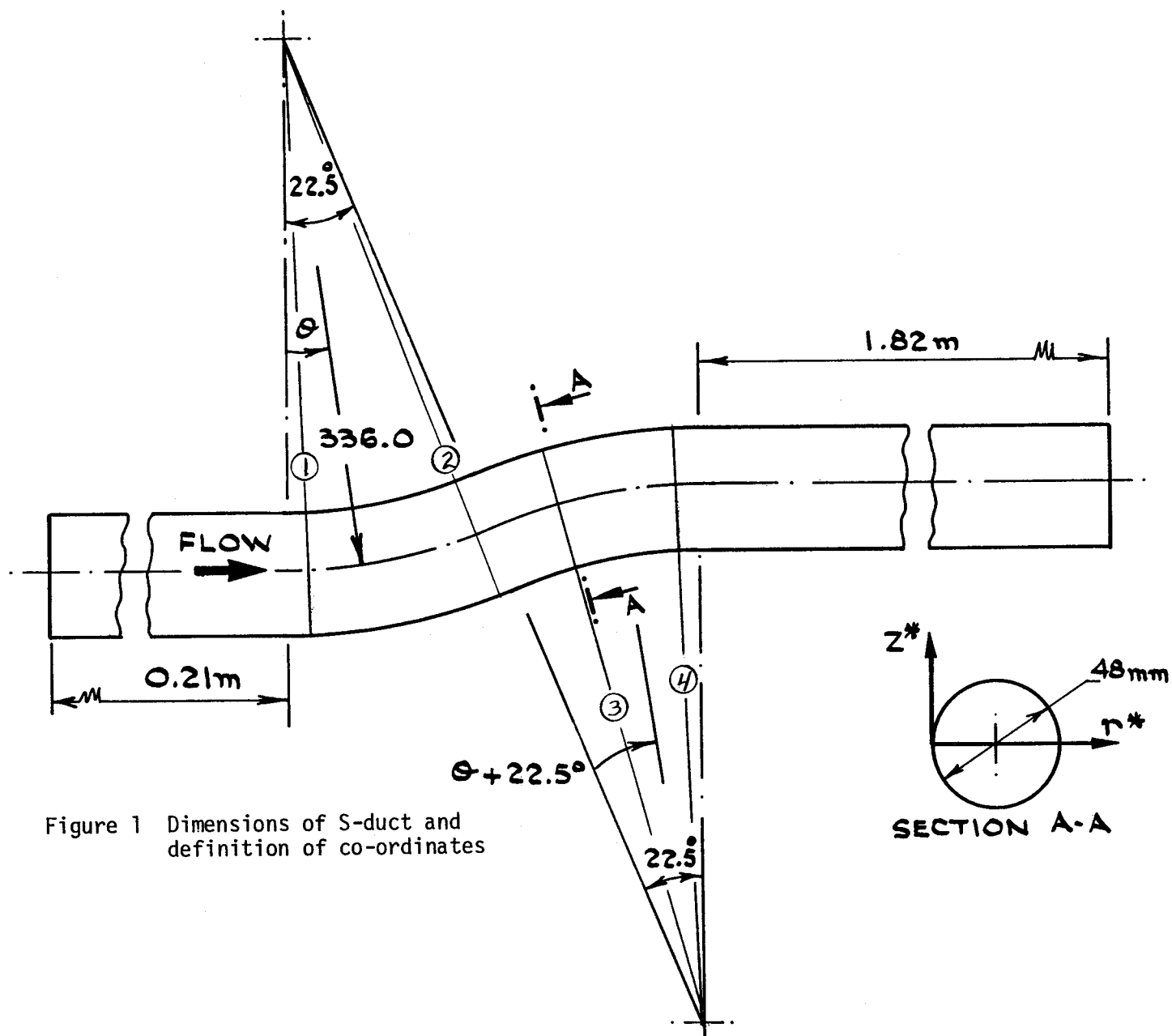


Figure 1 Dimensions of S-duct and definition of co-ordinates

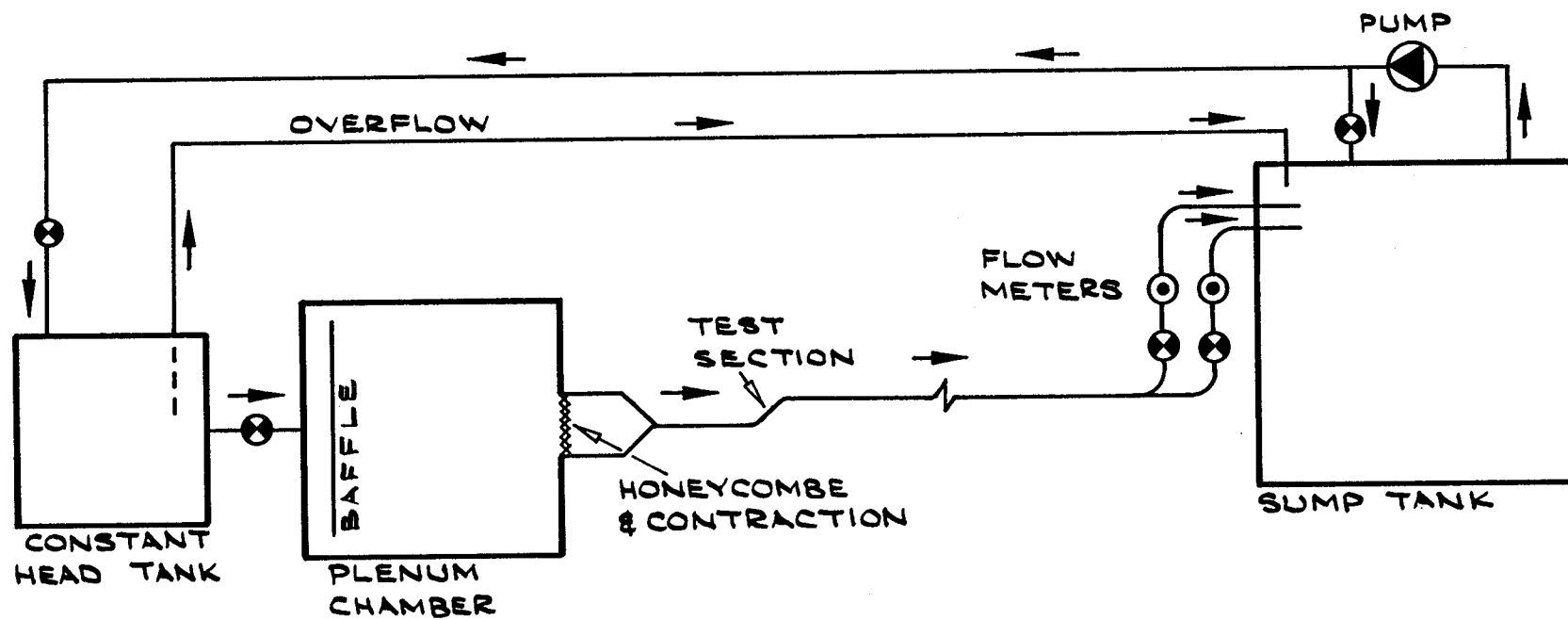


Figure 2 Plan view of water tunnel

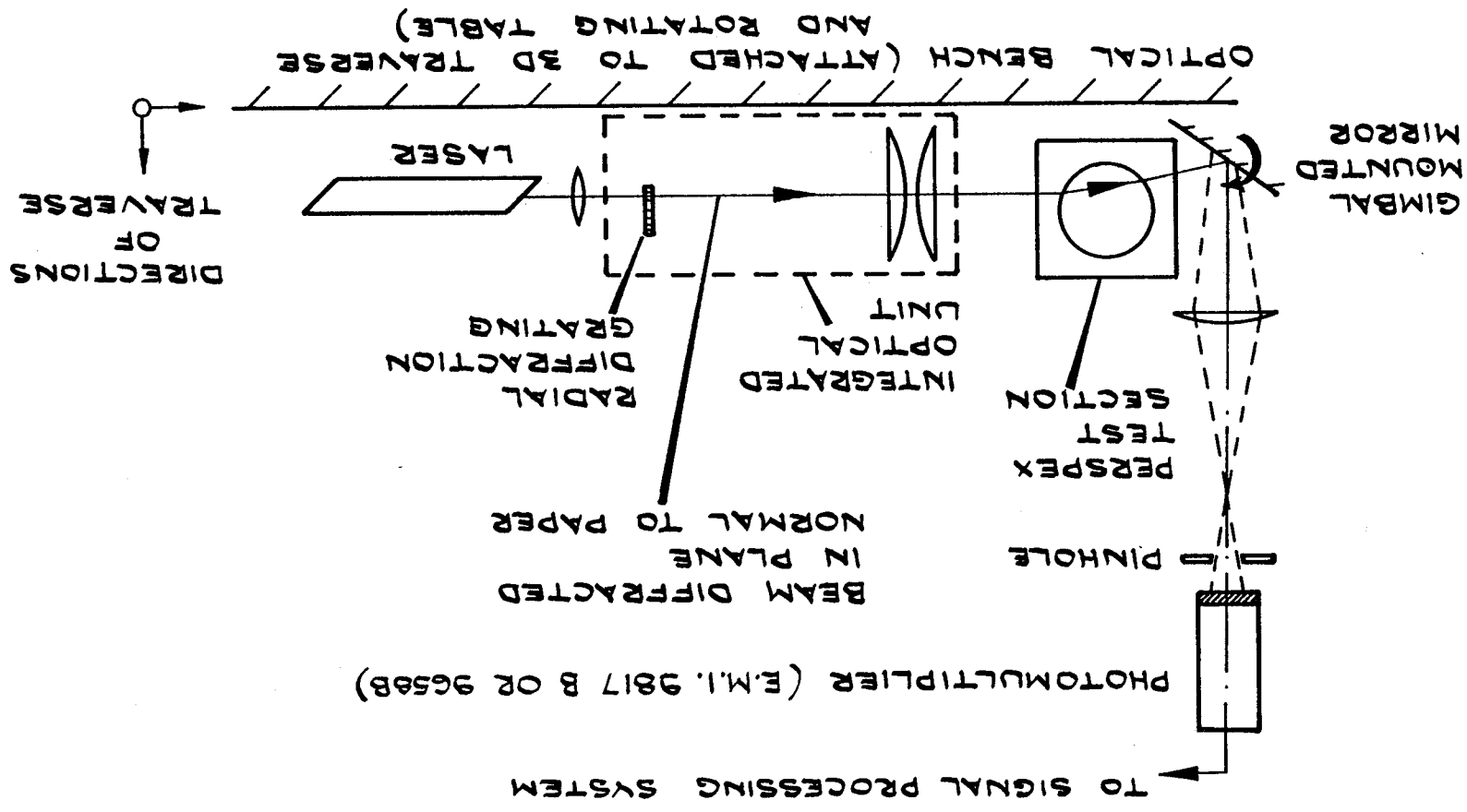


Figure 3(a) Optical arrangement of LDV for streamwise velocity measurements

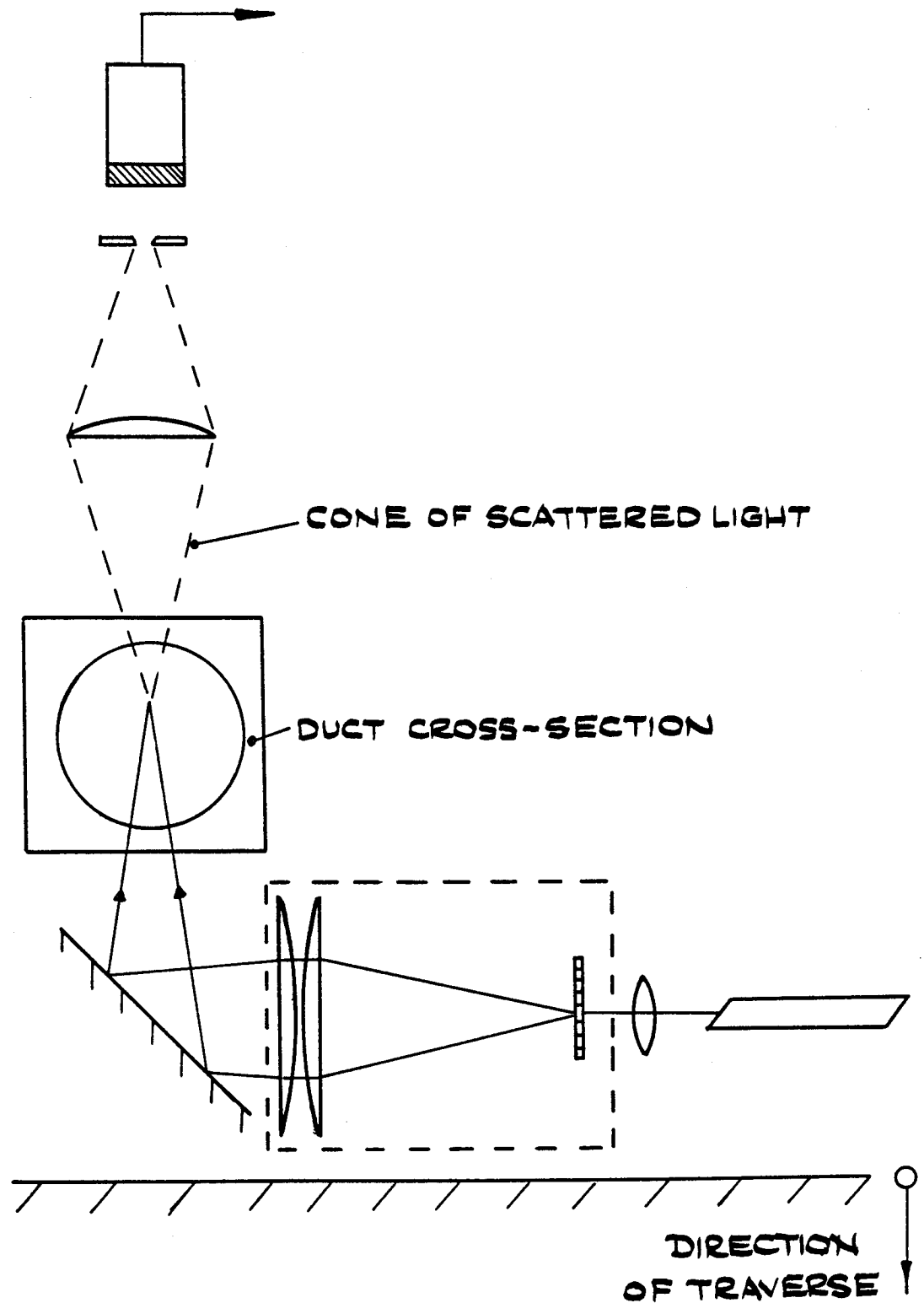


Figure 3(b) Optical arrangement of LDV for radial velocity measurements

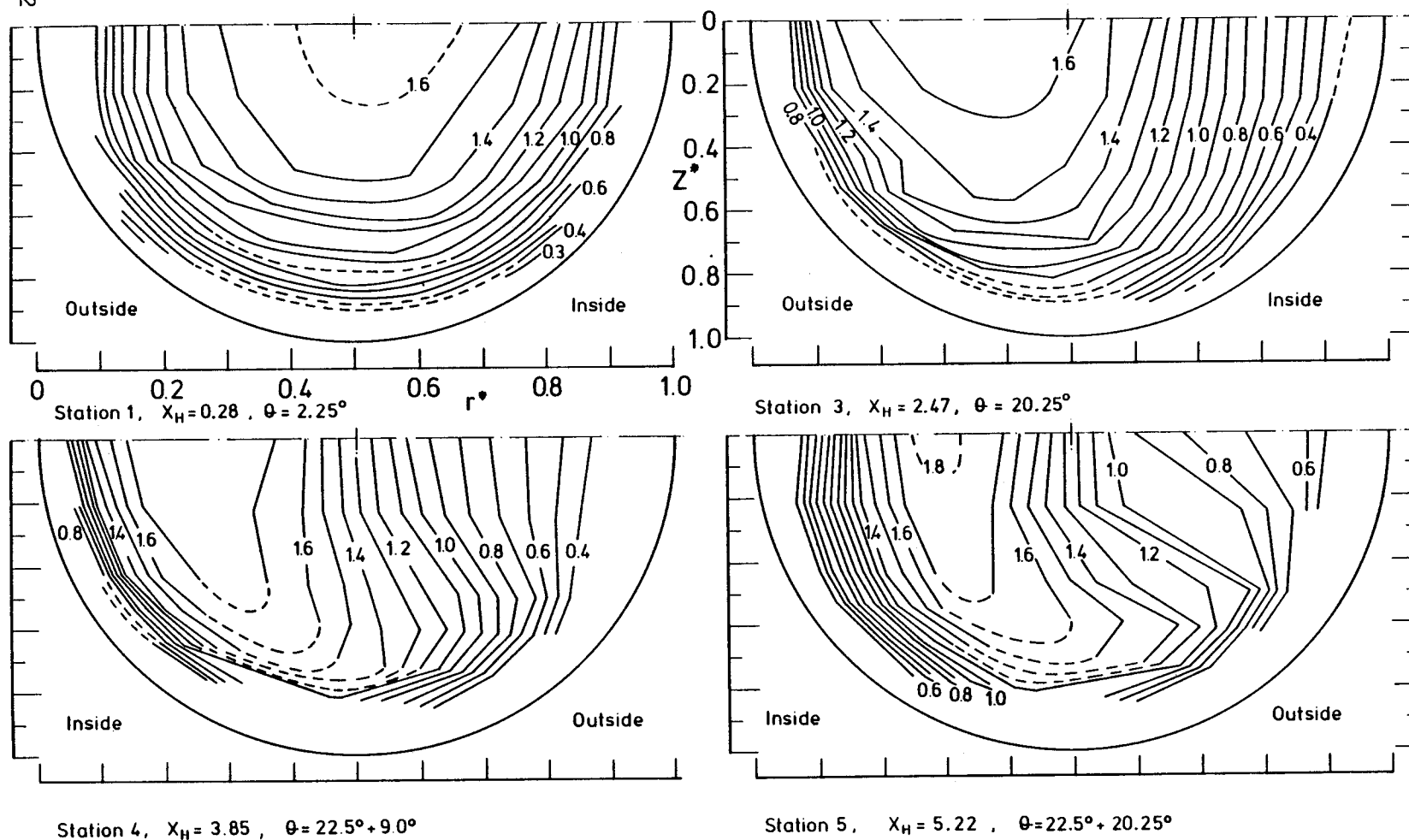


Figure 4 Laminar flow: isotachs of U/V_b at successive streamwise stations

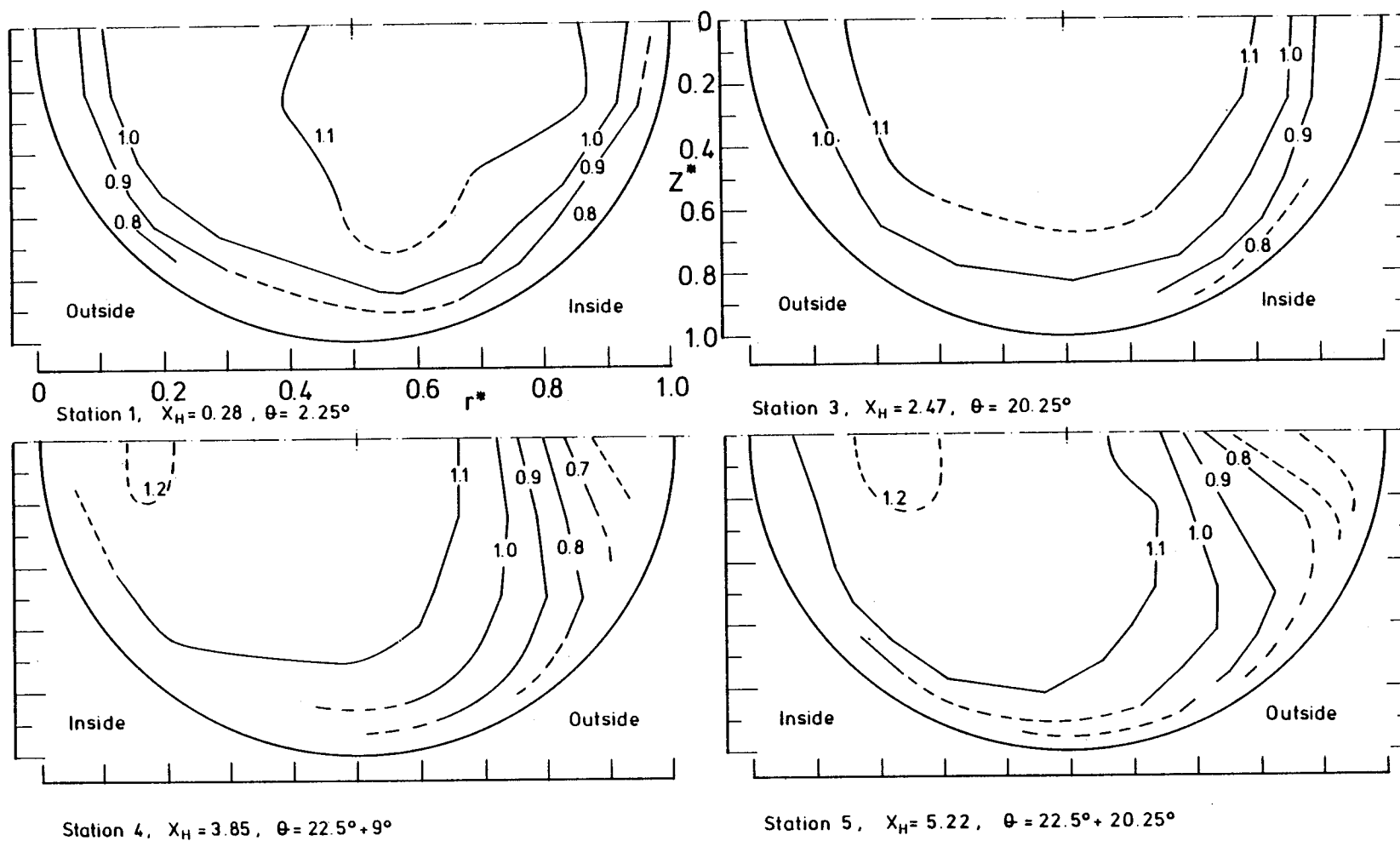


Figure 5 Turbulent flow: isotachs of \bar{U}/V_b at successive streamwise stations

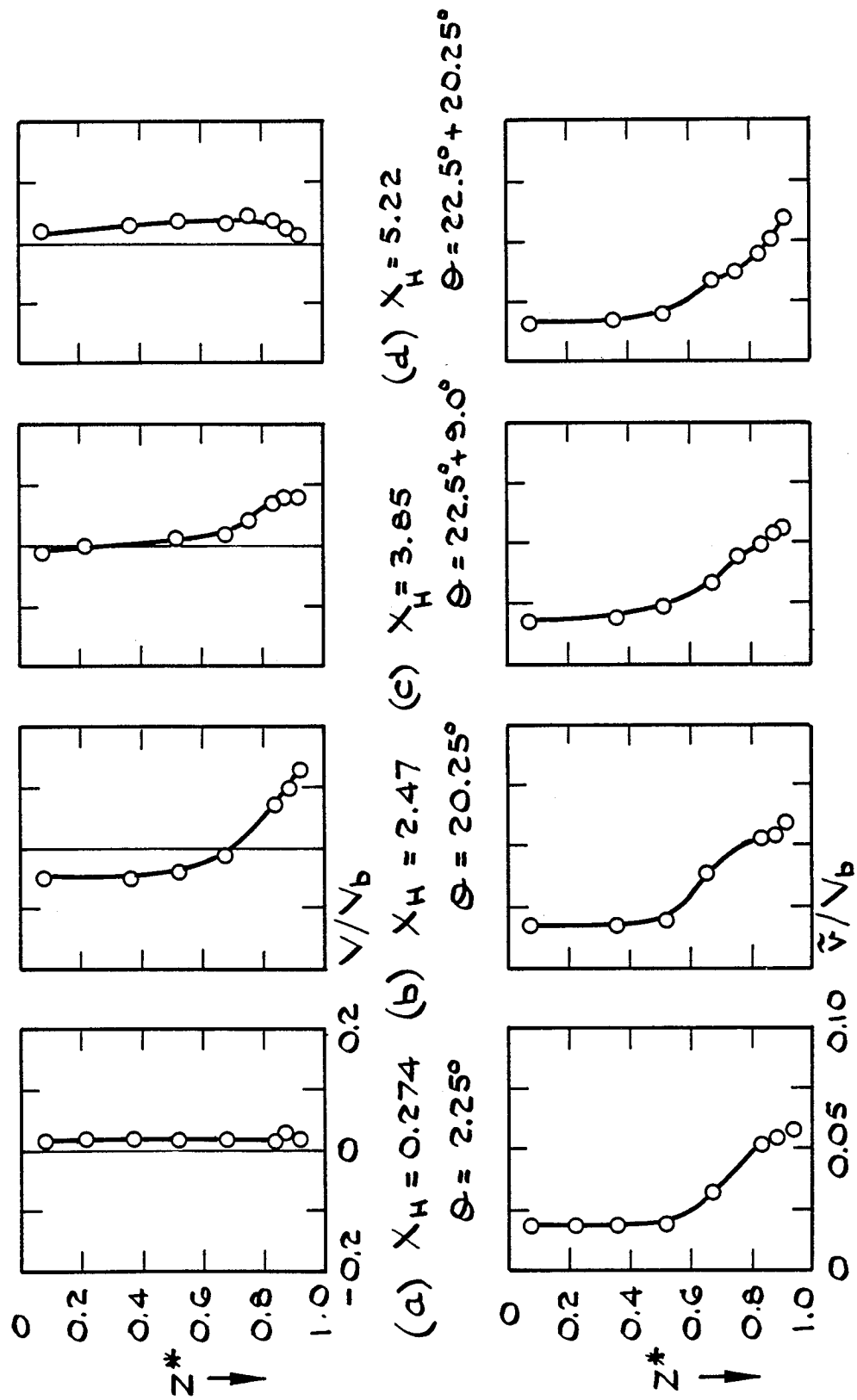
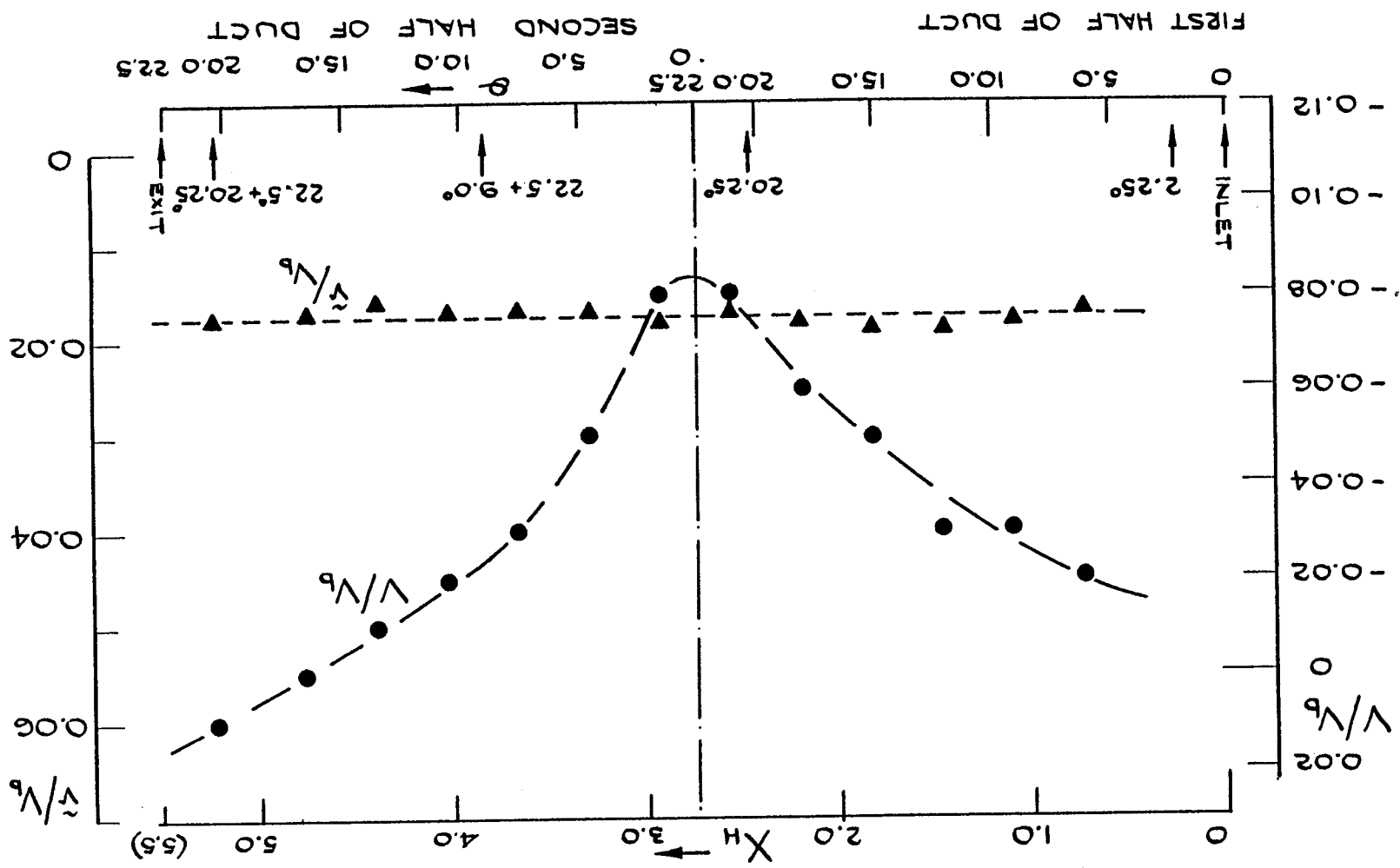


Figure 6 Turbulent flow: profiles of \bar{V}/V_b and \tilde{V}/V_b for $r^* = 0.5$ (n.b. V is positive in the positive r direction)

Figure 7 Turbulent flow: centre-line ($r^* = 0.5$, $z^* = 0.0$) development of mean and r.m.s. radial velocity



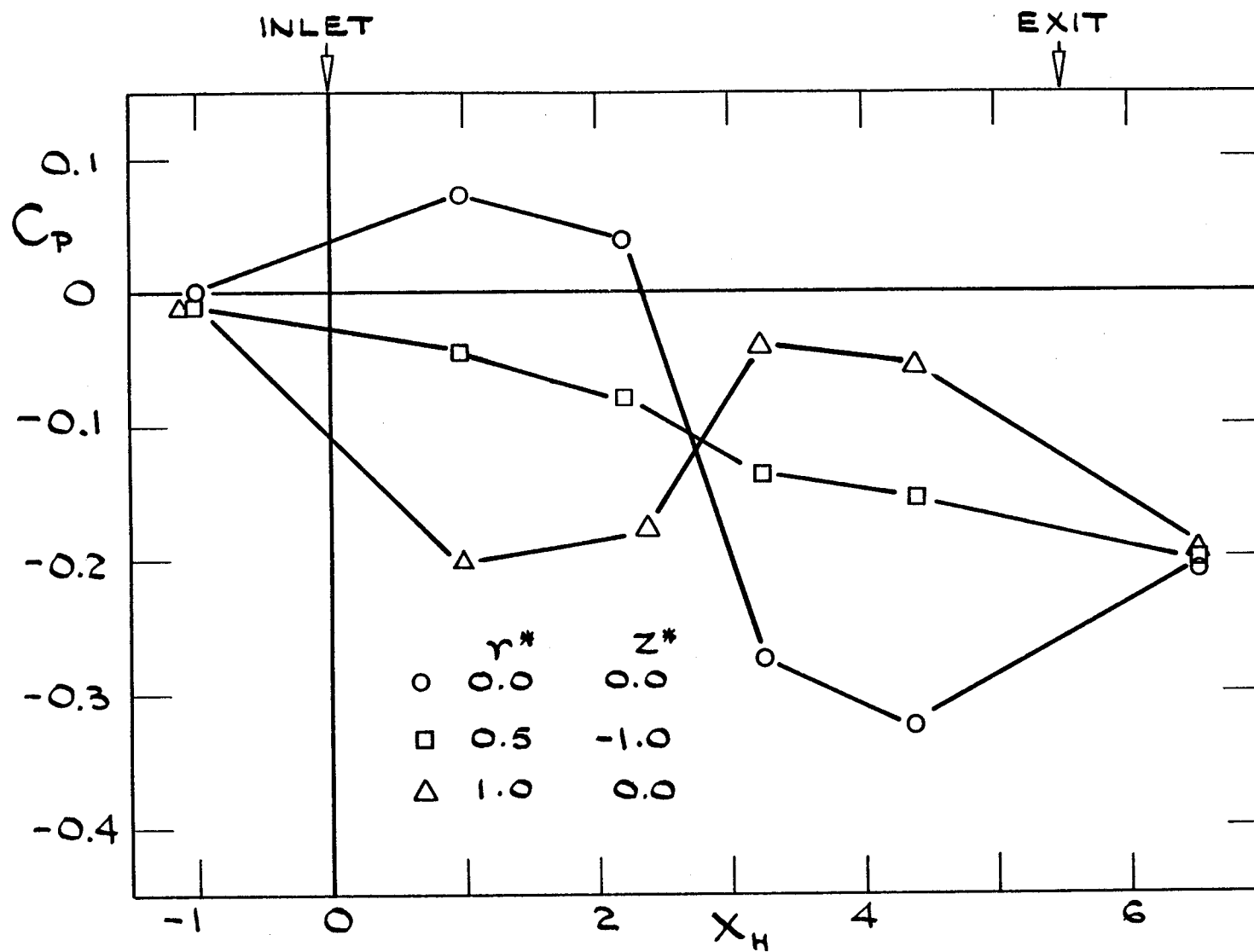


Figure 8 Turbulent flow: wall pressure distribution

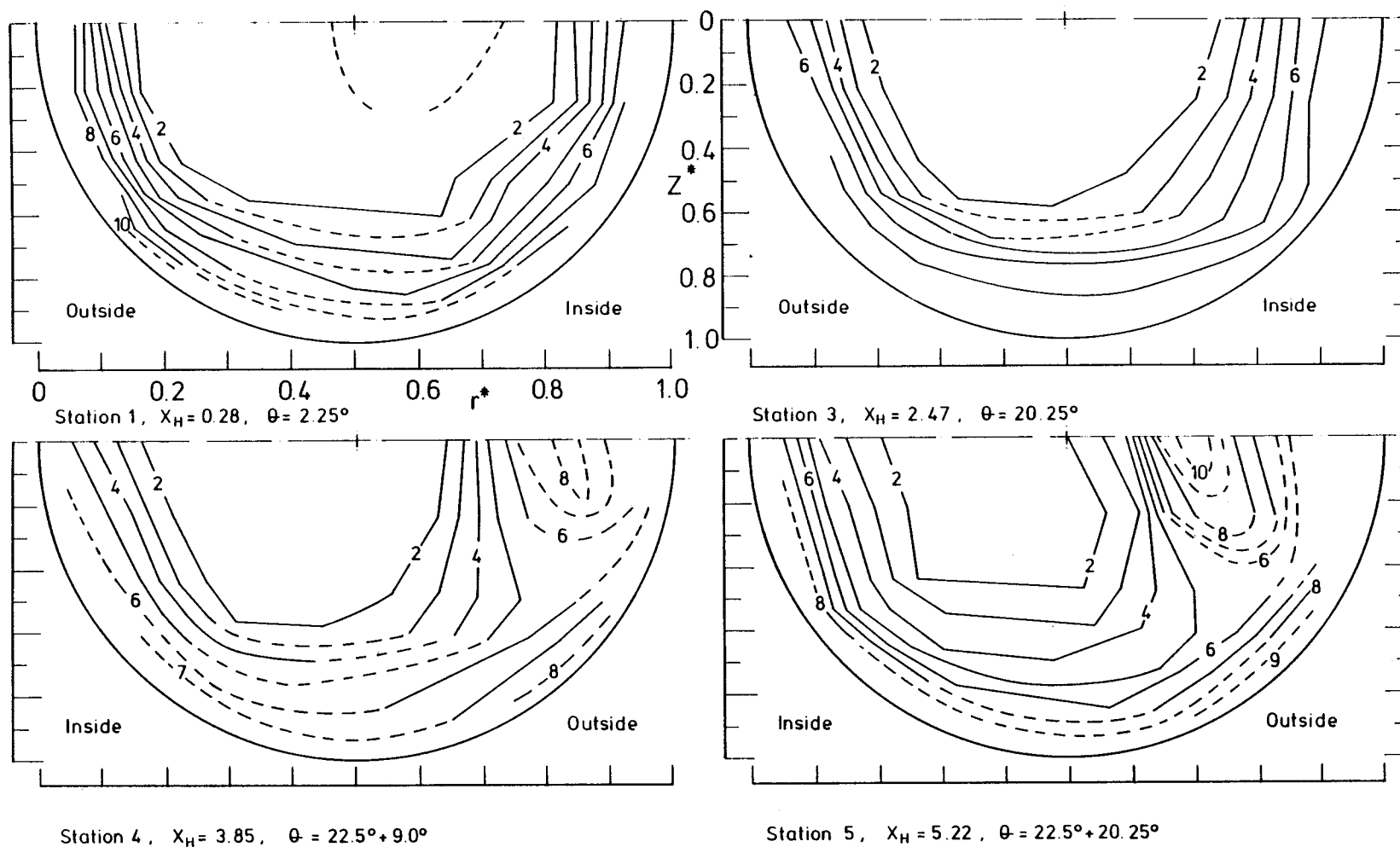


Figure 9 Turbulent flow: contours of \tilde{u}/V_b ($\times 100$) at successive streamwise stations

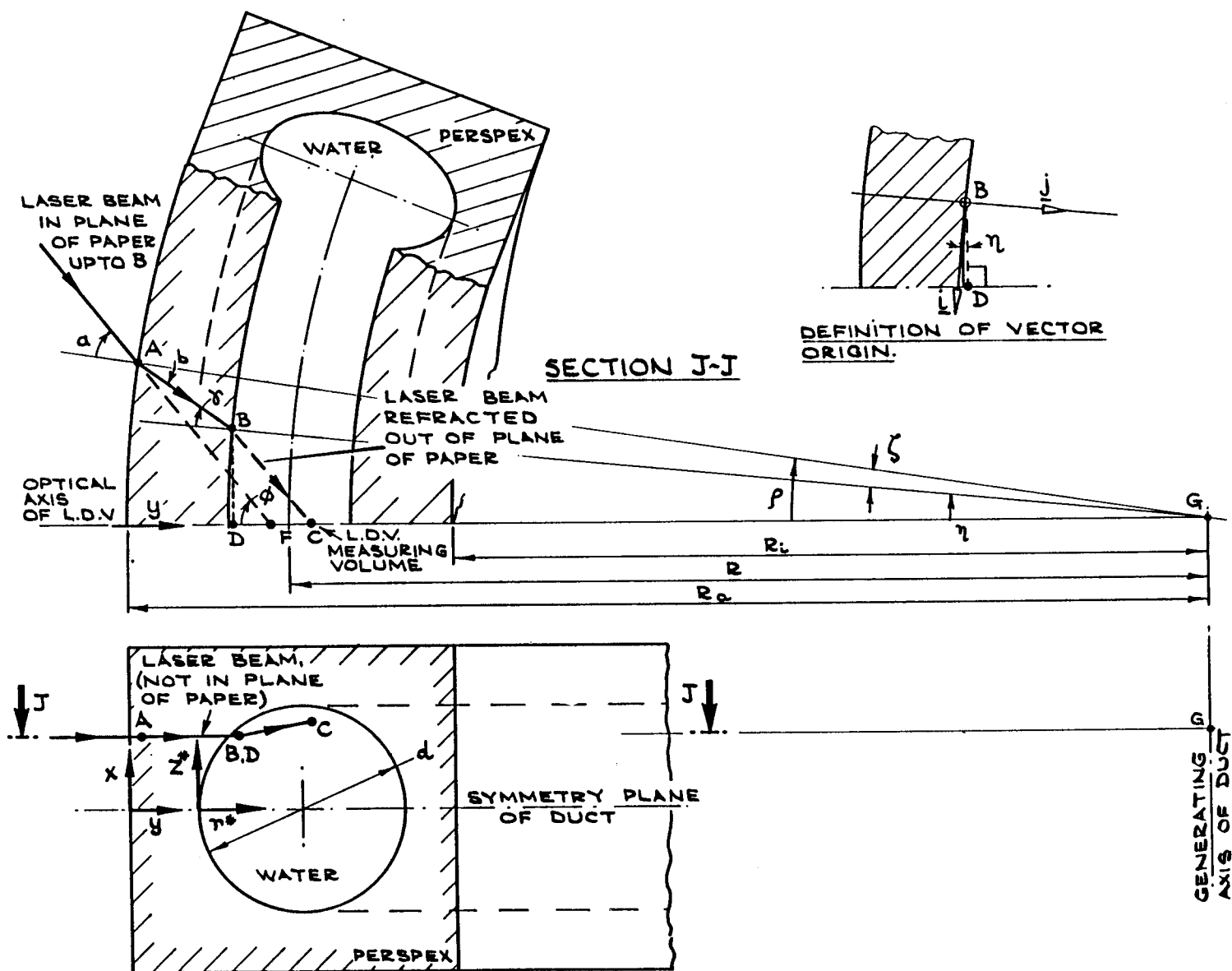


Figure A1 Path of laser beam through first half of S-duct (streamwise velocity measurement)

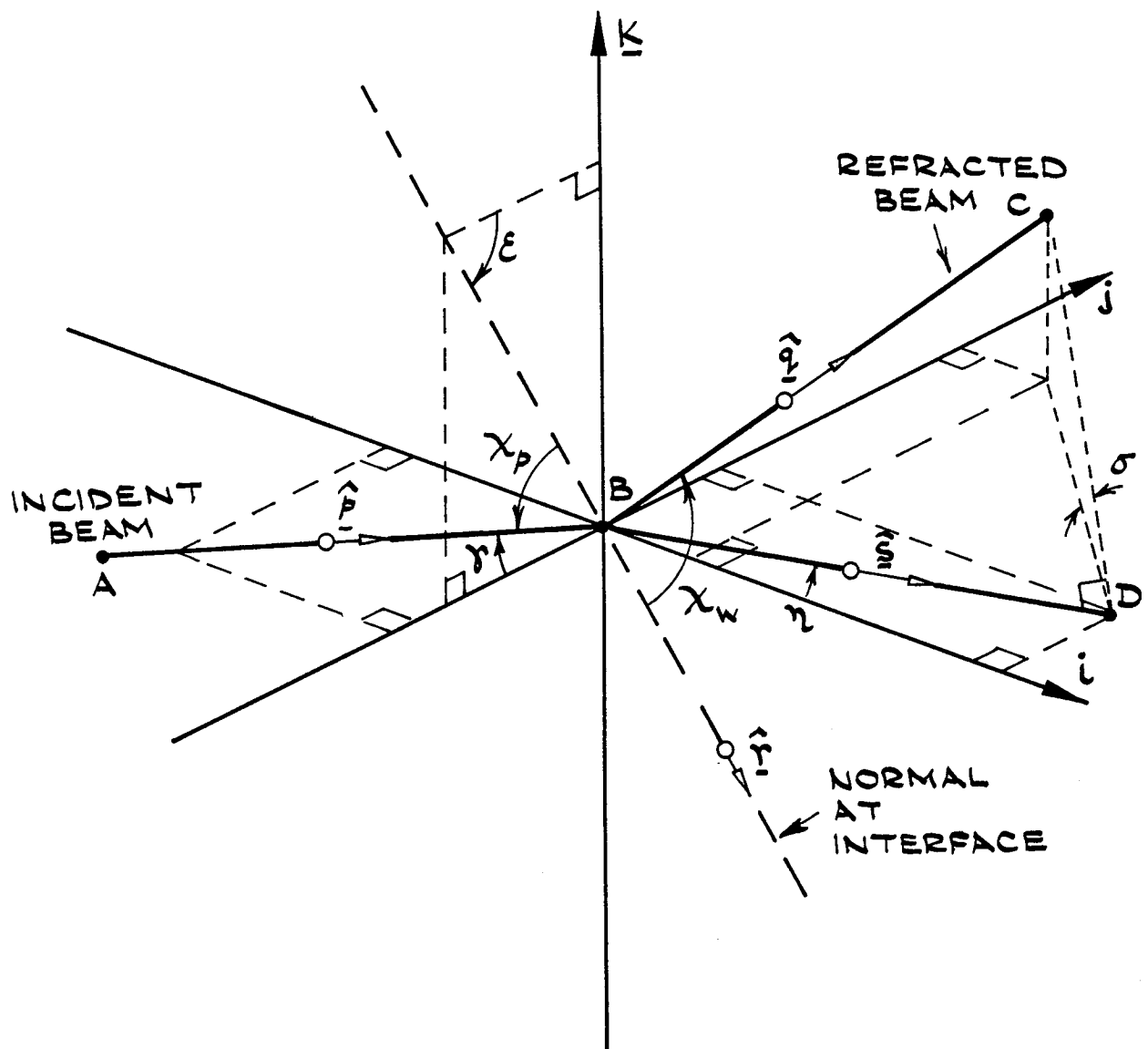


Figure A 2 Refraction of beam at point B for the first half of S-duct.
Refer also to the definition of the vector origin, figure A 1

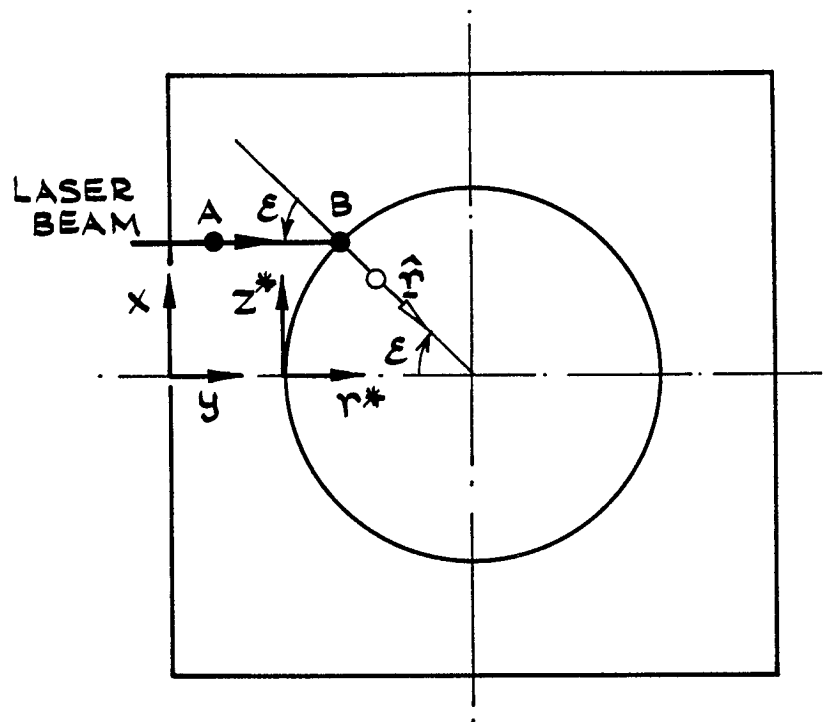


Figure A3 Section across duct, passing through point B
(both first and second halves of S-duct)

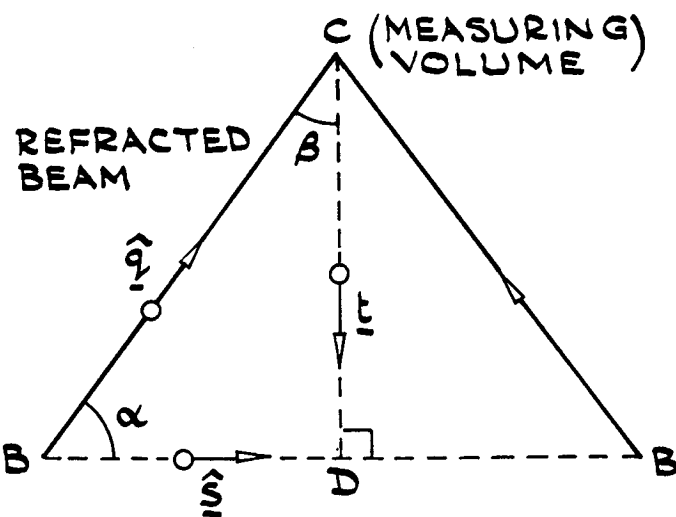


Figure A4 Beam path in water

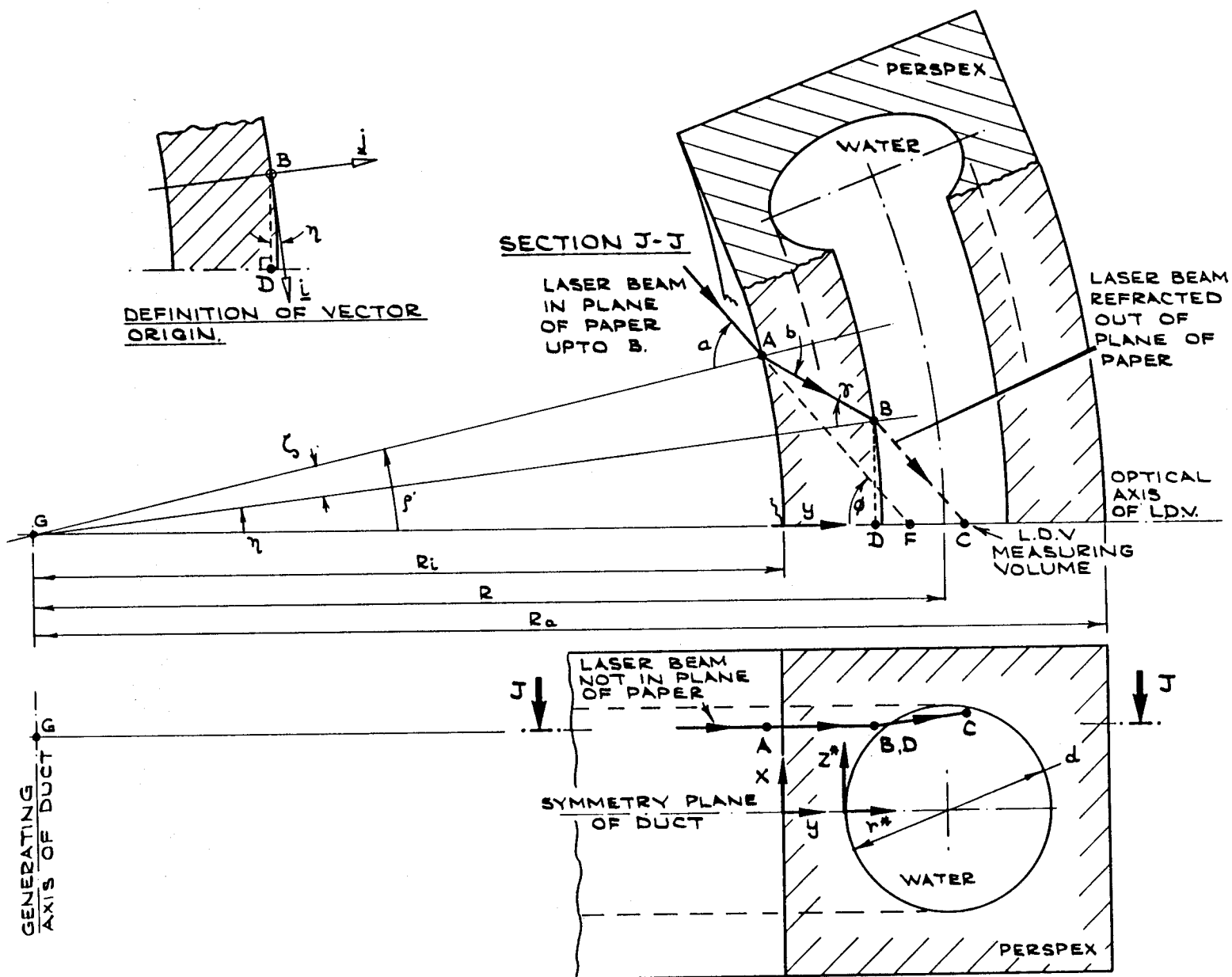
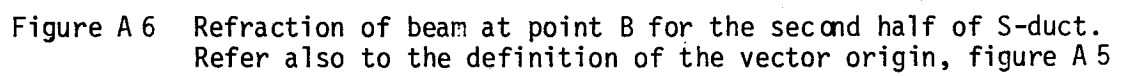


Figure A5 Path of laser beam through second half of S-duct (streamwise velocity component measurement)



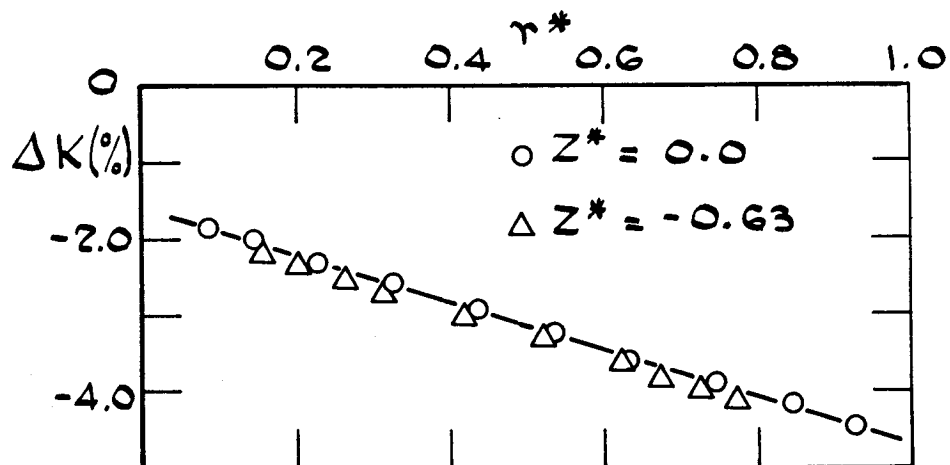


Figure A7a. - Calculated change in velocimeter transfer constant (ΔK) as a function of radial position (r^*).

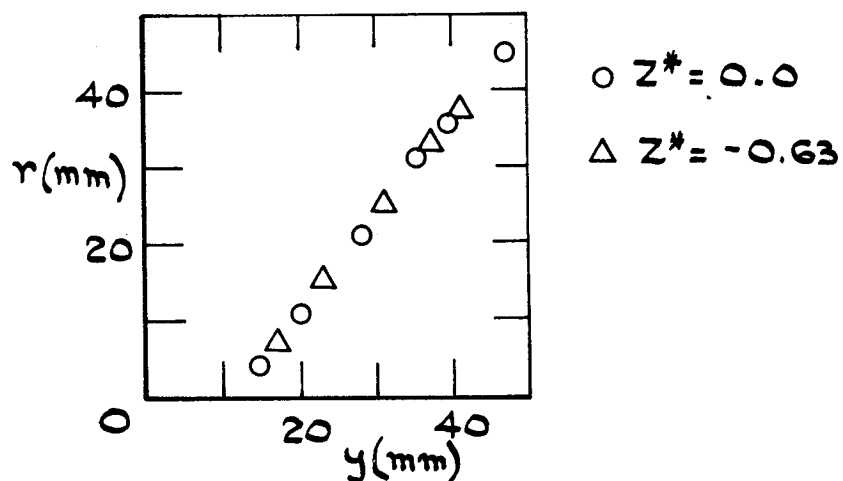


Figure A7b. - Calculated radial displacement (r) of beam intersection as a function of traverse co-ordinate, y .

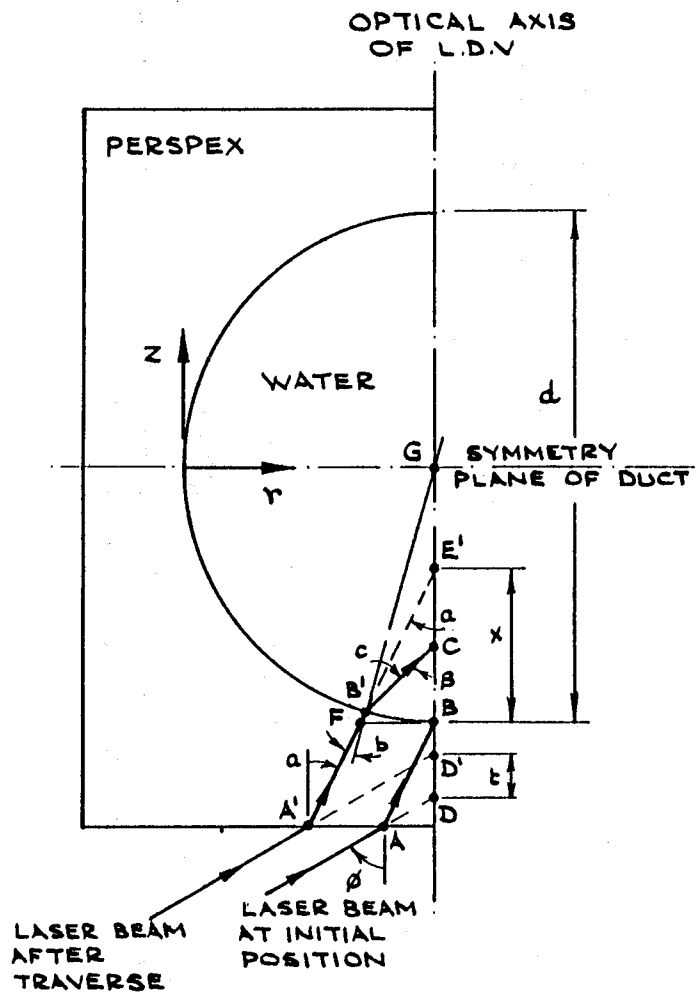


Figure B1 Path of laser beam for V-component velocity measurement. Intersection volume formed below plane of symmetry

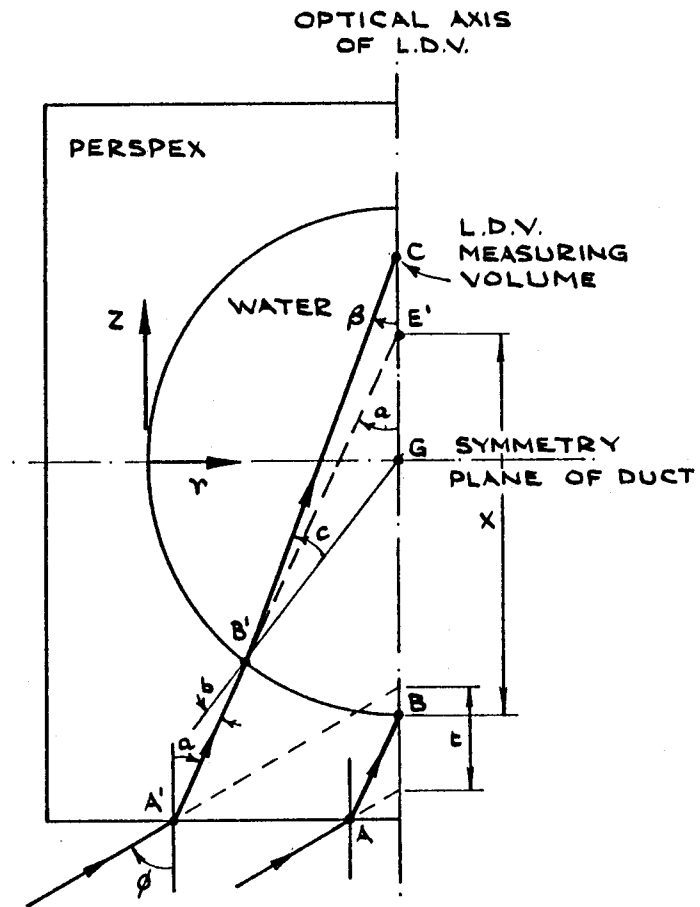


Figure B2 Path of laser beam for V-component velocity measurement. Intersection volume formed above plane of symmetry.

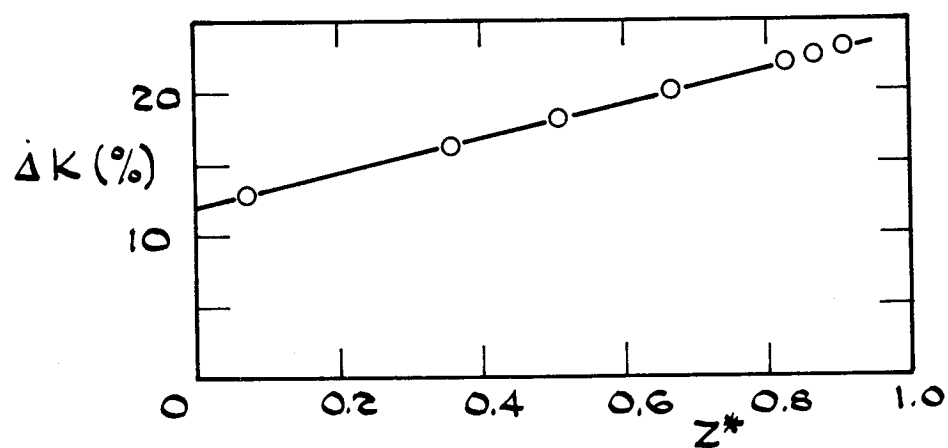


Figure B 3 Calculated change in velocimeter transfer constant (ΔK) as a function of altitude (z^*)

1. Report No. NASA CR-3759		2. Government Accession No.		3. Recipient's Catalog No.	
4. Title and Subtitle Developing Flow in S-Shaped Ducts II - Circular Cross-Section Duct				5. Report Date February 1984	
				6. Performing Organization Code	
7. Author(s) A. M. K. P. Taylor, J. H. Whitelaw, and M. Yianneskis				8. Performing Organization Report No. FS/82/7	
				10. Work Unit No.	
9. Performing Organization Name and Address Imperial College of Science and Technology Department of Mechanical Engineering Exhibition Road London SW7 2BX, England				11. Contract or Grant No. NASW-3435	
				13. Type of Report and Period Covered Contractor Report	
12. Sponsoring Agency Name and Address National Aeronautics and Space Administration Washington, D.C. 20546				14. Sponsoring Agency Code 505-40-02 (E-1939)	
15. Supplementary Notes Final report. Project Manager, Warren R. Hingst, Aerodynamics and Engine Systems Division, NASA Lewis Research Center, Cleveland, Ohio 44135.					
16. Abstract Laser-Doppler velocimetry was used to measure the laminar and turbulent streamwise flow in a S-duct (Reynolds numbers 790 and 48 000; Dean numbers 299 and 18 100) formed by two 22.5° sectors of a circular bend with ratio of mean radius of curvature to hydraulic diameter of 7.0. The wall pressure distribution and one component of cross-stream velocity are also reported for the turbulent flow case. The boundary layers near to the inlet of the duct were about 25 percent of the hydraulic diameter in the laminar flow and varied around the periphery of the pipe between 10 percent and 20 percent in turbulent flow. Pressure-driven secondary flows develop in the first half of the S-duct which are attenuated and reversed in the second half as a consequence of the change in the sense of curvature. There is, however, for both Reynolds numbers, a region near the outer wall of the second half of the duct where the sign of the radial vorticity results in an enforcement of the secondary flow which was established in the first half of the S-duct. The core flow (fluid with streamwise velocity greater than 0.90 of the local maximum) migrates, for both Reynolds numbers, to the outside wall of the first half and lies towards the inside wall of the second half of the S-duct at the outlet. The thinner inlet boundary layers in the turbulent flow give rise to weaker secondary motion, however.					
17. Key Words (Suggested by Author(s)) Secondary flow Laser-Doppler velocimetry Ducts - Intake systems				18. Distribution Statement Unclassified - unlimited STAR Category 34	
19. Security Classif. (of this report) Unclassified		20. Security Classif. (of this page) Unclassified		21. No. of pages 56	
				22. Price* A04	